Ann. Inst. H. Poincaré D
Comb. Phys. Interact. 10 (2023), 159–204
DOI 10.4171/AIHPD/133

A study in $\mathbb{G}_{\mathbb{R},\geq 0}(2,6)$: from the geometric case book of Wilson loop diagrams and SYM $N = 4$

Susama Agarwala and Siân Zee Fryer

Abstract. We study the geometry underlying the Wilson loop diagram approach to calculating scattering amplitudes in Supersymmetric Yang Mills (SYM) $N = 4$. In particular, we study the smallest non-trivial multi-propagator case, consisting of 2 propagators on 6 vertices. We do this by translating the integrals of the theory to the combinatorics of the positive geometry each diagram represents, specifically identifying the positroid cells defined by each diagram and the homology of the subcomplex they collectively generate in $\mathbb{G}_{\mathbb{R},\geq 0}(2,6)$. We verify the conjecture that the spurious singularities of the volume functional *do* all cancel on the codimension 1 boundaries of these cells, in this case. We also show that how the spurious singularities cancel is actually much more complicated than previously understood. The direct calculation laid out in this paper identifies many intricacies and artifacts of the geometry of Wilson loop diagram that need further study.

1. Introduction

In this paper, we consider the geometric underpinnings of the scattering amplitudes of SYM $N = 4$ theory. Recently, the amplituhedron established an association between the SYM $N = 4$ theory and polytopes in the positive Grassmannians [12]. There, the on shell scattering amplitudes in SYM $N = 4$ are computed using BCFW diagrams. Conjecturally, the amplituhedron is tiled by the image (under multiplication by $\mathcal{Z}$) of the $4k$-dimensional cells of $\mathbb{G}_{\mathbb{R},\geq 0}(k,n)$ that correspond to the BCFW diagrams in the physical theory [12, 22]. There is a large body of work connecting BCFW diagrams to plabic graphs (see [21, 22] and [10, Chapter 4]), and from there to a stratification by positroid cells of a subspace of $\mathbb{G}_{\mathbb{R},\geq 0}(k,n)$ (see [28]).

Another approach to understanding the amplitudes of SYM $N = 4$ theory is via the study of MHV amplitudes. This is the approach taken in this paper, where the MHV amplitudes are represented by Wilson loop diagrams. In both these cases the scattering amplitudes are given in terms of volumes of polytopes. The actual volume

2020 Mathematics Subject Classification. Primary 81Q60; Secondary 14M15, 13F60.
Keywords. SYM $N = 4$, positive Grassmannians, Deodhar decomposition.

is a function of the external particle data, here represented by a matrix $\mathcal{Z}$. Unlike the BCFW diagrams, the Wilson loop gives the entire scattering amplitude [8]. The calculations done in this paper consider N^kMHV diagrams in twistor space [13, 14, 24] which we call *Wilson loop diagrams*. These are the equivalent of Feynman diagrams for the theory in the twistor space setting.

One of the ultimate goals of this program is to understand the geometry underlying the Wilson loop diagrams, and the space they are mapped to by the external data matrices $\mathcal{Z}$, just as in the amplituhedron. Because of their common origin, one would expect to find that the geometries of these two closely related representations of the same physical theory would be very similar. However, this is proving significantly difficult to show. For instance, in [16, 19] the authors detail explicit difficulties in relating the geometry defined by the Wilson loop diagrams to the amplituhedron. This paper lays a foundation for exploring how these two geometries are related by systematically understanding the structure of the CW complex in $\mathbb{G}_{\mathbb{R},\geq 0}(k,n)$ defined by the Wilson loop diagrams (those corresponding to N^kMHV diagrams on n points).

For instance, one of the biggest difference between the Wilson loop diagrams and the BCFW setting is the dimension of the geometric spaces they represent. Specifically, BCFW diagrams define $4k$-dimensional subspaces of the positive Grassmannian $\mathbb{G}_{\mathbb{R},\geq 0}(k,n)$. Here, we show that for $k=2$ and $n=6$, the Wilson loop diagrams define a 6-dimensional subspace of $\mathbb{G}_{\mathbb{R},\geq 0}(k,n)$, or conjecturally, a $3k$-dimensional subspace of the positive Grassmannian. Subsequent work has verified this conjecture [4, 23], and shown that if one includes the gauge vector that is necessary in the N^kMHV calculations (but not in the BCFW computations), one gets a $4k$-dimensional subspaces of the full Grassmannian $\mathbb{G}_{\mathbb{R}}(k,n+1)$, see [6].

As a renormalizable theory, the N^kMHV integrals of SYM $N=4$ has two types of singularities: physical singularities, or infrared singularities, and the spurious singularities, which should cancel in the sum of the integrals [20]. In this paper, we show that this cancellation occurs on the boundary of the *positive* geometry, i.e., in the 6-dimensional cells in $\mathbb{G}_{\mathbb{R},\geq 0}(2,6)$. Furthermore, we show that the folklore conjecture that these cancellations can be read off from the diagramatics of the Wilson loop diagrams is false. In particular, there are multiple diagrams that correspond to the same positroid geometry [3, 7], yet all of their integrals are needed in order to ensure the cancellation of spurious poles; some pairs of Wilson loop diagrams share a boundary, even if this is not apparent from the diagramatics; many of the cancellations are not pairwise cancellations, but come from a combination (in this case) of three integrals being added together; there are boundaries of the positive geometry that are not necessary for the cancellation of spurious singularities. It is this last observation in particular, which does not exist in the $k=1$ case, that makes the understanding of cohomology of the positive geometry of Wilson loop diagrams difficult. While subsequent work has shown that the codimension one spurious singularities do, in fact,

vanish on the boundaries of the $3k$ positroid cells in $\mathbb{G}_{\mathbb{R},\geq 0}(k,n)$ (see [5]), understanding which boundaries these singularities correspond to, and thus a more general understanding of the cohomology of this space is still elusive.

In this paper our goals are twofold. The first goal is to explicitly compute the details of a small and concrete example, namely the case $k = 2, n = 6$, the smallest multi-propagator interaction in this theory. In doing this calculation, we discover a multitude of intricate interactions that both leads to interesting mathematical questions and makes the generalization of the results of this paper difficult. Contemporaneous to the development of this paper, others have computed the full details of the cancellation of spurious singularities in the case of $k = 1, n \geq 5$ worked out, see [19]. The second goal is to survey some of the general theory of Wilson loop diagrams, Feynman integrals, and the applications of tools from total positivity (e.g., Le diagrams, vertex-disjoint path systems) to these questions in a way that is accessible to both mathematicians and physicists.

The main results of this paper are as follow. First, by applying the techniques of total positivity, we verify that all admissible N^2MHV diagrams on 6 points yield positroid cells of dimension 6 (= $3k$). A complete list of the these positroids is given in Table 1. With this data in hand, we are able to obtain a complete description of the physically-interesting boundaries of the Wilson loop diagrams (the "boundary diagrams") in terms of the positroid cell structure on $\mathbb{G}_{\mathbb{R},\geq 0}(2,6)$ (see Section 4.11 for precise definitions):

Proposition 1.1 (Proposition 4.15). *B is a 5-dimensional positroid cell parametrized by the boundary diagram $\partial_{p,v}(W)$ of some admissible Wilson loop diagram W and corresponds to a simple pole of the associated integral $\mathcal{I}(W)(\mathcal{Z}_*)$, if and only if B lies on the boundary of 6-dimensional positroid cells in $\mathbb{G}_{\mathbb{R},\geq 0}(2,6)$ that are parametrized by at least two distinct Wilson loop diagrams.*

Note that one needs at least two different diagrams, not two different positroid cells. Furthermore, the number two is a lower bound. That is, boundaries may be shared by multiple diagrams and cells. Furthermore, not every 5-dimensional positroid in $\mathbb{G}_{\mathbb{R},\geq 0}(2,6)$ corresponds to a cell parametrized by a boundary diagram. This can be seen by direct computation (in this "small" case, there are only 50 cells of dimension 5 to consider), or by computing the homology of the space $\mathcal{W}(2,6)$ generated by the cells corresponding to the Wilson loop diagrams:

Theorem 1.2 (Theorem 4.20). *The homology groups of $\mathcal{W}(2,6)$ are as follows:*

$$H_i(\mathcal{W}(2,6)) = \begin{cases} \mathbb{R} & \text{if } i \in 0,5; \\ 0 & \text{else.} \end{cases}$$

As noted above, it is conjectured that the singularities appearing in the computation of the scattering amplitude should all cancel out on the codimension one boundaries of the cells associated to Wilson loop diagrams. In Section 5, we verify this for $k = 2, n = 6$, as summarized in the following theorem.

Theorem 1.3 (Theorem 5.1). *Let W be an admissible Wilson loop diagram with 2 propagators and 6 external particles. Let Σ' be any 5-dimensional boundary of the 6-dimensional cell $\Sigma(W)$ associated to W. Then*

$$\sum_{\substack{\partial_{p,v}(W')=\Sigma' \\ W' \text{ admiss}}} \operatorname*{Res}_{\Delta_{p,v}(W')\to 0} \mathcal{I}(W')(\mathcal{Z}_*) = 0. \tag{1}$$

In particular, the direct calculations of this paper reveal intricacies and obstacles that will carry forward as one adds more propagators and interacting particles. The CW structure of $\mathcal{W}(2,6)$ is far more complicated than can be easily inferred from the Wilson loop diagrams themselves, and can only be truly studied with the help of tools from total positivity such as Le diagrams. In order to implement a general proof that the codimension one singularities cancel for general k and n, one needs further classification and understanding of the properties of the factors of the polynomial that appears in the denominator of $I(W)$. For further discussion of this, see Section 6.

This paper is organized as follows. In Section 2, we define Wilson loop diagrams from a purely combinatorial point of view. We outline the tools and results that we use from the theory of total positivity, including positroid cells, Le diagrams, and vertex-disjoint path systems. Finally, we show how to identify the positroid cell associated to a given Wilson loop diagram. In Section 3, we recall the integrals associated to Wilson loop diagrams and give a brief discussion of how these integrals correspond to the holomorphic Wilson loop. We also include a worked example of evaluating the integral associated to a Wilson loop to illustrate the computations involved, and to motivate later sections.

In Section 4, we consider the specifics of N^2MHV diagrams on 6 points, and give a full description of the positroid cells they define. In Section 4.3, we show that the conjectured graphical device for identifying and comparing boundaries of the positroid cells associated to Wilson loop diagrams is (Graphical Prompt 4.11) is not sufficient to understand the full boundary structure of said cells. In Example 4.14 we give an explicit example of where the Graphical Prompt fails. Also, Example 4.5 identifies a boundary of a Wilson loop diagram cell that is shared by positroid cells with no corresponding Wilson loop diagram. We use these facts to compute the homology of the CW complex generated by the N^2MHV and Wilson loop diagrams on 6 points and the $NMHV$ diagrams on $n \geq 5$ point.

In Section 5, we show that all singularities of the integrals associated to N^2MHV Wilson loop diagrams on 6 points cancel in the sum over all diagrams. Furthermore,

the cancellations for these diagrams all occur, as expected, on the codimension one boundaries of the cells. This behavior has been conjectured for general k and n, but had not previously been verified even for $k = 2, n = 6$ due to the difficulties in identifying all shared codimension one boundaries from the Wilson loop diagrams alone.

Section 6 summarizes the observations about the structure of the general geometry of Wilson loop diagrams uncovered by the calculations in this paper. These observations need to be better understood in order to generalize the result of this paper to general k and n. Some of the necessary steps of this generalization have been completed in subsequent work, as outlined in this section.

2. Wilson loop diagrams

This section is an introduction to the combinatorics of Wilson loop diagrams for mathematicians. As such, we omit the derivation of the diagrams and associated integrals, and the precise definitions of the physical objects involved (see existing literature [1]), and focus on the diagrams themselves as combinatorial objects.

In Section 2.1, we establish the notation and conventions used in this paper. Section 2.2 describes the diagramatics of the Wilson loop diagrams themselves, Section 2.3 provides an overview of total positivity and some related combinatorial objects, and Sections 2.4 and 2.5 make precise the relationship between Wilson loop diagrams and total positivity.

2.1. Notation

Let $M_{\mathbb{R}}(k,n)$ denote the set of all $k \times n$ real matrices, and $M_{\mathbb{R},+}(k,n)$ the subset of those matrices whose maximal (i.e., $k \times k$) minors are strictly positive.

We represent the Grassmannian $\mathbb{G}_{\mathbb{R}}(k,n)$ as the set of all full rank $k \times n$ real matrices modulo the left action of $\mathrm{GL}_k(\mathbb{R})$; intuitively, these are $k \times n$ matrices with linearly independent rows, where two matrices are "the same" if we can get from one to the other by performing row operations.

Definition 2.1. A point in $\mathbb{G}_{\mathbb{R}}(k,n)$ is called *totally non-negative* if it can be represented by a matrix whose maximal minors (i.e., its $k \times k$ minors) are all nonn-egative. Denote the set of all totally non-negative points by $\mathbb{G}_{\mathbb{R},\geq 0}(k,n)$.

Let $[n]$ denote the interval $\{1, 2, \ldots, n\}$, and

$$\binom{[n]}{k} = \{I \subset [n] \mid |I| = k\}$$

the set of all k-subsets of $[n]$. Clearly $\binom{[n]}{k}$ is in bijection with the set of possible maximal minors of a $k \times n$ matrix. We write Δ_I for the minor with columns indexed by I, or $\Delta_I(A)$ for the value of the minor evaluated on a specific matrix A.

Each individual Wilson loop diagram encodes one piece of the calculation whose sum yields the scattering amplitude. The result of this calculation depends on the external data associated to each particle in the interaction.

Definition 2.2. An external particle of a Wilson loop diagram is denoted $Z \in \mathbb{R}^{4+k}$. Write Z^j to denote the j-th component of Z and Z^μ to denote the projection of the section Z onto its twistor component, i.e., onto the first four coordinates.

An n point Wilson loop diagram has n external particles and a gauge vector, and we collect this external data in a matrix as follows.

Definition 2.3. Write $\mathcal{Z}$ for the $n \times (k+4)$ matrix whose rows consist of the n vectors $Z_1, Z_2, \ldots, Z_n$ associated to the external particles. We restrict our attention to collections of particles in general position, and demand that the external data form matrices with positive maximal minors. In other works, $\mathcal{Z} \in M_{\mathbb{R},+}(n, 4+k)$. We may choose a *gauge vector* Z_* that is a point in a zero section of the line bundle of external particles. Denote by $\mathcal{Z}_* \in M_{\mathbb{R}}(n+1, 4+k)$ the matrix obtained by prepending Z_* above the first row of $\mathcal{Z}$.

We refer to these matrices $\mathcal{Z}_*$ as the matrices of external data. A standard convention throughout this paper is that objects with a star subscript include the gauge vector data, while those without a star subscript omit the gauge vector from consideration. As described in the introduction, there are often reasons for including or omitting the gauge from our calculations.

We also define a notation for certain 4×4 determinants which play an important role in calculations:

$$\langle abcd \rangle = \det(Z_a^\mu Z_b^\mu Z_c^\mu Z_d^\mu),$$

i.e., the determinant of the 4×4 matrix whose rows correspond to the external particles Z_a, Z_b, Z_c, and Z_d, each projected to their first four coordinates.

2.2. Wilson loop diagrams

We now discuss the Wilson loop diagrams combinatorially.

Definition 2.4. A *Wilson loop diagram* is a convex n-gon ($n \geq 4$) with k internal (wavy) lines called MHV propagators, each of which connects a pair of distinct polygon edges. See Figure 1 for an example of a Wilson loop diagram.

The vertices of the boundary polygon correspond to the external particles involved in the represented interaction. The location of the propagator endpoint on the polygon

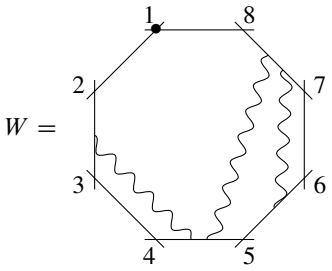

Figure 1. A Wilson loop diagram with 8 vertices and 3 propagators.

edge is not significant; if several propagators share an edge, by convention we arrange them in order to minimize the number of crossings.

Note that we have not yet put any restrictions on the behaviour of the propagators, e.g., excluding diagrams with crossing propagators. The underlying physics will impose certain conditions on the propagators; this is described in Section 2.4 below.

By labeling the vertices of the polygon, we obtain the following equivalent definition of a Wilson loop diagram:

Definition 2.5. A Wilson loop diagram (WLD) is comprised of a cyclically ordered set $(S, <) \subset [n]$ and a set of k pairs of elements of S. For ease of reference, we impose the following convention on the propagators:

$$\mathcal{P} = \{(i_1, j_1), \ldots (i_k, j_k) \mid i_r, j_r \in S; i_r <_1 j_r \text{ for all } r\},$$

where $<_1$ denotes the total order induced from $<$ by choosing some element of S (usually 1) to be the "first" element. We write $W = (\mathcal{P}, S)$ for the Wilson loop diagram, or (for simplicity) $W = (\mathcal{P}, n)$ when $S = [n]$.

The set S labels the boundary vertices of a convex n-gon, starting at the marked vertex and moving counterclockwise. This induces a labeling of the edges, where the i-th edge connects vertices i and $i + 1$ (or the successor of i, if $S \neq [n]$). The ordered pair $(i_r, j_r) \in \mathcal{P}$ corresponds to the propagator connecting edges i_r and j_r.

For example, the diagram in Figure 1 can also be written as $W = (\{(2,4),(4,7),(5,7)\},8)$.

Definition 2.6. 1. Given a propagator $p \in \mathcal{P}$, the *support* of p is the set

$$V_p = \{i_p, i_p + 1, j_p, j_p + 1\},$$

i.e., the endpoints of the two boundary edges that the propagator touches.

2. Given a set of propagators $Q \subset \mathcal{P}$, define $V_Q = \bigcup_{q \in Q} V_q$ to be the support of Q.

3. For a set of vertices $V \subset [n]$, write $\mathrm{Prop}(V) = \{p \in \mathcal{P} \mid V \cap V_p \neq \emptyset\}$ for the subset of propagators supported by V.

Definition 2.7. If $W = (\mathcal{P}, n)$ is a Wilson loop diagram, and $Q \subset \mathcal{P}$ a non-empty subset of its propagators, the *subdiagram* of W associated to Q is $W_Q = (Q, V_Q)$.

For ease of reference later, we impose an (arbitrary) naming convention for the propagators. Namely, given a Wilson loop diagram W with k propagators, label the propagators as $p_1, \ldots, p_k$, in the order they are first encountered while walking counterclockwise around W from the marked vertex. We use this convention unless indicated otherwise.

We now associate two matrices to each Wilson loop diagram, based on the ordering convention above. All work in this paper can be done under any other ordering convention.

Definition 2.8. Define a $k \times n$ matrix $\mathcal{C}(W)$ by placing indeterminates $c_{b,a}$ in some of its entries and 0s elsewhere, as follows:

$$\mathcal{C}(W)_{b,a} = \begin{cases} c_{b,a} & \text{if } a \in V_{p_b}; \\ 0 & \text{else.} \end{cases}$$

We will also want to consider the matrix $\mathcal{C}_*(W)$ obtained by prepending a column of 1s to $\mathcal{C}(W)$; in order to maintain column labeling consistency, we label the columns of $\mathcal{C}_*(W)$ from 0 to n. In other words,

$$\mathcal{C}_*(W)_{b,a} = \begin{cases} 1 & \text{if } a = 0; \\ c_{b,a} & \text{if } a \in V_{p_b}; \\ 0 & \text{else.} \end{cases}$$

In both matrices, the entries $c_{b,a}$ are real indeterminates.

Example 2.9. For the Wilson loop diagram $W = (\{(2,4),(4,7),(5,7)\}, 8)$ in Figure 1, the associated matrices $\mathcal{C}(W)$ and $\mathcal{C}_*(W)$ are

$$\mathcal{C}(W) = \begin{pmatrix} 0 & c_{1,2} & c_{1,3} & c_{1,4} & c_{1,5} & 0 & 0 & 0 \\ 0 & 0 & 0 & c_{2,4} & c_{2,5} & 0 & c_{2,7} & c_{2,8} \\ 0 & 0 & 0 & 0 & c_{3,5} & c_{3,6} & c_{3,7} & c_{3,8} \end{pmatrix},$$

$$\mathcal{C}_*(W) = \begin{pmatrix} 1 & 0 & c_{1,2} & c_{1,3} & c_{1,4} & c_{1,5} & 0 & 0 & 0 \\ 1 & 0 & 0 & 0 & c_{2,4} & c_{2,5} & 0 & c_{2,7} & c_{2,8} \\ 1 & 0 & 0 & 0 & 0 & c_{3,5} & c_{3,6} & c_{3,7} & c_{3,8} \end{pmatrix}.$$

2.3. Positroids and Le diagrams

In recent years, the study of totally non-negative matrices and their associated combinatorics has emerged as an extremely useful tool for the study of scattering amplitudes in SYM $N = 4$; see for example [7, 12, 21]. In this section we give a short introduction to this non-negative viewpoint, and outline the key definitions and techniques we make use of in this paper.

For the purposes of this paper, a *representable matroid* is any collection $\mathcal{B} \subseteq \binom{[n]}{k}$ which can be "represented" by an element of $\mathbb{G}_{\mathbb{R}}(k,n)$, i.e., there exists some $A \in \mathbb{G}_{\mathbb{R}}(k,n)$ such that for all $B \in \binom{[n]}{k}$,

$$\Delta_B(A) \neq 0 \iff B \in \mathcal{B}.$$

Following the language of matroid theory, we will refer to the elements of $\mathcal{B}$ as the *bases* of the matroid.

Definition 2.10. A *positroid* is a representable matroid $\mathcal{B}$ which can be represented by an element of $\mathbb{G}_{\mathbb{R},\geq 0}(k,n)$.

This definition induces a stratification of $\mathbb{G}_{\mathbb{R},\geq 0}(k,n)$ into *positroid cells*: for each positroid $\mathcal{B}$, define

$$\mathcal{S}_{\mathcal{B}} = \{A \in \mathbb{G}_{\mathbb{R},\geq 0}(k,n) \mid \Delta_B(A) \neq 0 \text{ if and only if } B \in \mathcal{B}\},$$

i.e., the set of points in $\mathbb{G}_{\mathbb{R},\geq 0}(k,n)$ which represent $\mathcal{B}$.

These definitions were introduced the foundational 2006 preprint [28] by Postnikov. The positroid stratification of $\mathbb{G}_{\mathbb{R},\geq 0}(k,n)$ defines a CW complex such that the boundary of each cell is homeomorphic to a sphere [30, Theorem 1.1]. In other words, $\mathbb{G}_{\mathbb{R},\geq 0}(k,n)$ is homeomorphic to a closed ball [17], the positroids partition $\mathbb{G}_{\mathbb{R},\geq 0}(k,n)$ into convex open cells of dimension $0 \leq d \leq k(n-k)$, the closure of a cell of dimension d is the union of that cell with finitely many cells of dimension $\leq d-1$, and explicit attaching maps have been constructed; see, e.g., [29, Theorem 6.2].

Remark 2.11. If we are only interested in which postroid cells lie on the boundary of a given cell, and not in the precise attaching map data, we may consider the face poset of this complex instead. Specifically: the positroid cell $\mathcal{S}_{\mathcal{B}'}$ is contained in the boundary of the cell $\mathcal{S}_{\mathcal{B}}$ if and only if the there is an inclusion $\mathcal{B}' \subset \mathcal{B}$ of the bases.

Positroids have many nice combinatorial properties, see for example [9, 17, 28]. While the matrices in this paper are small enough that it is easy to compute their minors by hand (and we will often use this method when considering the cell complex structure), examining long lists of bases is often unilluminating. We therefore introduce Le diagrams (Definition 2.12) as a convenient method of labeling the positroid

cells, and describe the method of vertex-disjoint path systems (Theorem 2.14) for passing between the list of bases defining a positroid and its Le diagram.

Definition 2.12. A *Le diagram* is a Young diagram where each box contains either a $+$ or a 0 symbol, subject to the rule that if a box contains a 0 then at least one of the following holds:

- every box to its left (in the same row) also contains a 0; *or*
- every box above it (in the same column) also contains a 0.

For example,

$+$	0	$+$	0
$+$	0	$+$	$+$

$+$	0	$+$	$+$
0	0		

$+$	$+$	$+$	$+$
$+$	$+$	$+$	

are all Le diagrams, while

$+$	$+$	$+$	$+$
$+$	0	$+$	

0	$+$
$+$	0

are not.

The positroids in $\mathbb{G}_{\mathbb{R},\geq 0}(k,n)$ are in bijection with the Le diagrams that fit inside a $k \times (n-k)$ rectangle, i.e., have at most k rows and at most $n-k$ columns [28, Theorem 6.5].

Remark 2.13. The dimension of a positroid cell is simply the dimension of the open ball it is homeomorphic to. Given a positroid cell, its dimension can easily be read from the corresponding Le diagram: it is precisely the number of $+$ squares appearing in the Le diagram.

There is also an algorithm to reconstruct the set $\mathcal{B}$ of non-zero minors from the Le diagram, as we now describe. Given a Le diagram L, construct its associated graph $\Gamma(L)$ as follows.

1. Label each step along the southeast border of L with the numbers $1, 2, \ldots, n$. (Note that if L has fewer than k rows, or fewer than $(n-k)$ columns, some of these steps will lie on the bounding rectangle; see Figure 2.)
2. Place a vertex in each $+$ square of L, and an additional vertex next to each row and column label.
3. Join any two consecutive vertices in the same row with an arrow directed leftwards, and any two consecutive vertices in the same column with an arrow directed downwards.

See Figure 2 for an example. It follows directly from the Le property that $\Gamma(L)$ is planar, i.e., two arrows can only meet at a vertex.

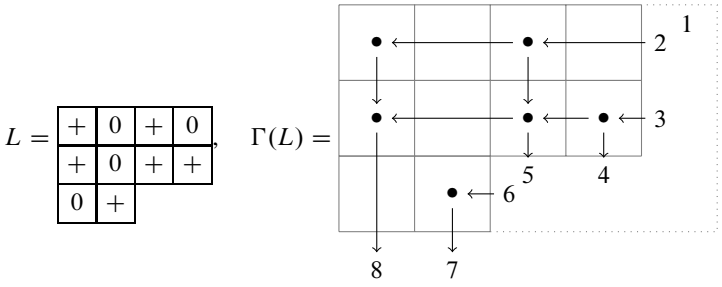

Figure 2. Constructing $\Gamma(L)$ from L in $\mathbb{G}_{\mathbb{R},\geq 0}(3,8)$.

Write S for the set of source vertices in the diagram (i.e., the vertices attached to row labels), and T for the set of target vertices (column labels). A *path* in $\Gamma(L)$ is any path from a vertex $s \in S$ to a vertex $t \in T$ along these directed arrows, as first defined in [28, Section 6]. Two paths are called *vertex-disjoint* if they do not have any vertices in common.

Let $I = \{i_1, \ldots, i_r\}$ be a subset of the row labels, and $J = \{j_1, \ldots, j_r\}$ a subset of the column vertices. A *vertex-disjoint path system* for (I, J) is a collection of paths

$$i_1 \to j_1,\ i_2 \to j_2,\ \ldots,\ i_r \to j_r,$$

which are pairwise vertex-disjoint.

Theorem 2.14. *Let L be a Le diagram specifying a cell in $\mathbb{G}_{\mathbb{R},\geq 0}(k,n)$, and construct its graph $\Gamma(L)$ as above. Then B is a basis for the positroid corresponding to L if and only if $|B| = k$ and $(S\backslash B, T \cap B)$ admits a vertex-disjoint path system.*

Proof. Combine [15, Theorem 5.6] and [18, Theorem 4.2]. ∎

Note that in earlier work, [28, Section 6], the author defines a boundary measure that translates between Le diagrams and networks parameterizing $\mathbb{G}_{\mathbb{R},\geq 0}(kn)$, and [31] gives a formula to compute the associated Plücker coordinates via vertex disjoint oriented cycles. While this is an equivalent way to determine the bases associated to a Le diagram, it is a distinct algorithm from that we use in this paper.

Example 2.15. For the Le diagram in Figure 2, we have $S = \{2, 3, 6\}$ and $T = \{1, 4, 5, 7, 8\}$. Then for example, $B = \{4, 5, 6\}$ is a basis for this positroid, since

$$S\backslash B = \{2, 3\}, \quad T \cap B = \{4, 5\},$$

and there is a vertex-disjoint path system $2 \to 5$, $3 \to 4$ in $\Gamma(L)$. On the other hand, $\{3, 4, 5\}$ is *not* a basis, since there is no vertex-disjoint path system from $\{2, 6\}$ to $\{4, 5\}$ in $\Gamma(L)$.

Notation 2.16. We will often drop the set notation for bases where this will not cause any confusion, i.e., write 456 for $\{4, 5, 6\}$.

For small examples in particular, vertex-disjoint path systems provide an effective way of listing all of the bases of a positroid without writing down an explicit matrix belonging to that positroid. Conversely, given a list of bases for a positroid, we can use Theorem 2.14 to reconstruct the corresponding Le diagram; this allows us to start with a Wilson Loop diagram and construct its Le diagram via the matrix $\mathcal{C}(W)$.

Recall that the cell structure on the positroids of $\mathbb{G}_{\mathbb{R},\geq 0}(k,n)$ can be seen in its face poset (ordered by inclusion). It is important to emphasize that these inclusions *cannot* always be read directly from the Le diagrams, as the following example demonstrates.

Example 2.17. In $\mathbb{G}_{\mathbb{R},\geq 0}(2,4)$, consider

$$A_1 = \begin{pmatrix} 1 & 0 & 0 & -a \\ 0 & 1 & 0 & b \end{pmatrix}, \quad A_2 = \begin{pmatrix} 1 & 0 & -c & -\alpha c \\ 0 & 1 & d & \alpha d \end{pmatrix}, \quad a, b, c, d, \alpha > 0$$

A_1 belongs to the positroid $\mathcal{S}_{\mathcal{B}_1}$ with $\mathcal{B}_1 = \{12, 14, 24\}$, while A_2 belongs to $\mathcal{S}_{\mathcal{B}_2}$ with $\mathcal{B}_2 = \{12, 13, 14, 23, 24\}$. So we certainly have $\mathcal{B}_1 \subseteq \mathcal{B}_2$, but there is no obvious relation between the Le diagrams:

$$L(\mathcal{S}_{\mathcal{B}_1}) = \begin{array}{|c|c|}\hline + & 0 \\ \hline + & 0 \\ \hline \end{array}, \quad L(\mathcal{S}_{\mathcal{B}_2}) = \begin{array}{|c|c|}\hline 0 & + \\ \hline + & + \\ \hline \end{array}.$$

Thus, we use Le diagrams as a convenient method of labeling positroids and calculating their dimension, and lists of bases when examining the cell structure.

2.4. Admissible Wilson loop diagrams

Thus far, we have not put any conditions on the behavior of the Wilson loop diagrams. It turns out that restricting our attention to the physically interesting ones (the *admissible* diagrams, Definition 2.19) yields matrices which also have interesting positivity conditions.

Fix a matrix of external data $\mathcal{Z}_*$, as described in Section 2.1. By Cramer's rule, each matrix $\mathcal{C}(W)$ defines a unique kernel of the matrix $\mathcal{Z}_*^\mu$. In [7], the first author and Amat show that solving the equation

$$\mathcal{C}_*(W) \cdot \mathcal{Z}_*^\mu = \mathbf{0} \tag{2}$$

for the entries $c_{b,a}$ of $\mathcal{C}_*(W)$ yields expressions that can be written in terms of certain minors of $\mathcal{Z}_*^\mu$, as we now describe. (The significance of equation (2) is discussed following Theorem 2.20.)

Definition 2.18. For a propagator $p_b = (i_b, j_b)$, and supporting vertex $a \in V_{p_b}$, define $\sigma_{b,a}$ to be the determinant formed by replacing the vector Z_a^μ in the determinant $\langle i_b\ (i_b+1)\ j_b\ (j_b+1)\rangle$ with the gauge vector Z_*^μ, i.e.,

$$\sigma_{b,a} = \langle Z_{i_b}^\mu \dots Z_*^\mu \widehat{Z_a^\mu} \dots Z_{j_b+1}^\mu \rangle.$$

Let $\mathcal{C}_*(W)(\mathcal{Z}_*)$ be the matrix obtained from $\mathcal{C}_*(W)$ by replacing each $c_{b,a}$ with

$$\frac{\sigma_{b,a}}{\langle i_b\ (i_b+1)\ j_b\ (j_b+1)\rangle}, \quad 1 \leq b \leq k,\ a \in V_{p_b}. \tag{3}$$

It follows from Cramer's rule that $C_*(W)(\mathcal{Z}_*) \cdot \mathcal{Z}_*^\mu = \mathbf{0}$ [7, (4)]. Thus, $\mathcal{C}_*(W)(\mathcal{Z}_*)$ is exactly the matrix that solves equation (2), for fixed external data $\mathcal{Z}_*$. See Example 3.3 for a worked example of computing $\mathcal{C}_*(W)(\mathcal{Z}_*)$.

We are interested in Wilson loop diagrams that define positroid cells in the correct Grassmannian, i.e., in $\mathbb{G}_{\mathbb{R},\geq 0}(k,n)$. To this end, we give the following definition.

Definition 2.19. A Wilson loop diagram $W = (\mathcal{P}, n)$ is called *admissible* if it satisfies the following conditions:

1. $n \geq |\mathcal{P}| + 4$;
2. there does not exist a (non-empty) subset of propagators $Q \subseteq \mathcal{P}$ such that $|V_Q| < |Q| + 3$;
3. W has no crossing propagators.

It is more illuminating to see examples of Wilson loop diagrams which *fail* to be admissible; some examples are listed in Figure 3.

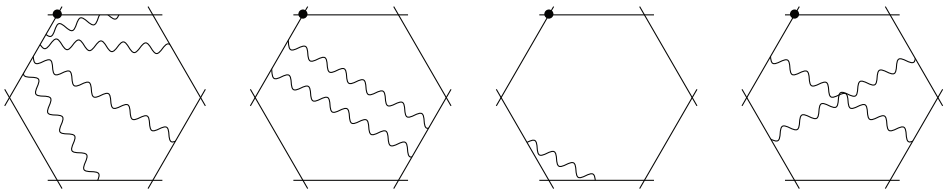

Figure 3. Examples of diagrams which *fail* to be admissible.

The following result makes precise the relationship between the matrices associated to admissible Wilson loop diagrams and total positivity.

Theorem 2.20 ([7, Theorems 1.14 and 3.41]). *Let W be an admissible Wilson loop diagram with k propagators on n vertices, and $\mathcal{Z}_*$ a matrix of external data. Then*

1. *$\mathcal{C}_*(W)(\mathcal{Z}_*)$ is a matrix of full rank for any choice of external data $\mathcal{Z}_*$, i.e., it lies in $\mathbb{G}_{\mathbb{R}}(k, n+1)$;*
2. *$\mathcal{C}(W)$ defines a positroid (in the sense of Definition 2.10).*

Each admissible Wilson loop diagram thus corresponds to a subspace of $\mathbb{G}_{\mathbb{R}}(k, n+1)$: the space parametrized by the matrix $\mathcal{C}_*(W)$ (recall Definition 2.8).

Write $\mathcal{W}_*(k,n) \subset \mathbb{G}_{\mathbb{R}}(k,n+1)$ for the subspace of $\mathbb{G}_{\mathbb{R}}(k,n+1)$ parametrized by all of the admissible Wilson loop diagrams. Any matrix of external data $\mathcal{Z}_*$ induces a projection map from $\mathcal{W}_*(k,n)$ to a subspace of $\mathbb{G}_{\mathbb{R},\geq 0}(k,k+4)$:

$$\mathcal{Z}_*\colon \mathcal{W}_*(k,n) \to \mathbb{G}_{\mathbb{R},\geq 0}(k,k+4),$$
$$\mathcal{C}_*(W) \mapsto \mathcal{C}_*(W)\cdot \mathcal{Z}_*.$$

The integrals associated to the admissible Wilson loop diagrams (introduced in Section 3) define volumes on the spaces of the form $\mathcal{C}_*(W)\cdot\mathcal{Z}_*$, and it is these volumes which yield the scattering amplitude. The volume associated to the space $\mathcal{C}_*(W)\cdot\mathcal{Z}_*$ is defined by evaluating a rational function at the hyperplane that satisfies (2).

However, in this paper we focus not on the image $\mathcal{Z}_*(\mathcal{W}_*(k,n))$ but on the positive geometry of the space parametrized by the Wilson loop diagrams $C(W)$. In later sections, we show that many of the problems that arise in evaluating and interpreting the integrals can be resolved by close inspection of this preimage.

Remark 2.21. The space $\mathcal{Z}_*(\mathcal{W}_*(k,n))$ is conjectured to be the amplituhedron. See also [16] for a connection between $\mathcal{W}_*(k,n)$ and a geometric space called the amplituhedron squared.

For the rest of this paper, *we consider admissible Wilson loop diagrams only*.

2.5. Wilson loop diagrams and positroids

In this paper, we are interested in the geometry defined by the admissible Wilson loop diagrams. In other words, we wish to study the subspace of $\mathbb{G}_{\mathbb{R},\geq 0}(k,n)$ parametrized by matrices of the form $\mathcal{C}(W)$, making use of the CW structure coming from the positroid stratification of $\mathbb{G}_{\mathbb{R},\geq 0}(k,n)$. The underlying physical justification for taking this approach is given in Section 3; for now, we simply note that the volume forms associated to individual Wilson loop diagrams have singularities which are conjectured to cancel out in the final sum, and in order to verify this conjecture it suffices to study their behavior on the boundaries of the positroids appearing in Theorem 2.20.

In this section we introduce the definitions and notation which will allow us to make precise the object whose geometry we need to understand. In Sections 4 and 5, we verify that the singularities do indeed all cancel out in the case $k=2, n=6$.

Definition 2.22. Let W be an admissible Wilson loop diagram, and $\mathcal{B}(W)$ the bases set of the positroid defined by $\mathcal{C}(W)$. Define $\Sigma(W)$ to be the corresponding closure of the positroid cell in $\mathbb{G}_{\mathbb{R},\geq 0}(k,n)$, i.e.,

$$\Sigma(W) = \overline{\{A \in \mathbb{G}_{\mathbb{R},\geq 0}(k,n) \mid \Delta_I(A) \neq 0 \iff I \in \mathcal{B}(W)\}}.$$

Definition 2.23. Define $\mathcal{W}(k,n)$ to be the subspace of $\mathbb{G}_{\mathbb{R},\geq 0}(k,n)$ consisting of the union of the closures of the positroid cells associated to admissible diagrams, i.e.,

$$\mathcal{W}(k,n) = \bigcup_{\substack{W \text{ admiss.} \\ n \text{ verts, } k \text{ props}}} \overline{\Sigma(W)}.$$

For the remainder of this paper, we restrict our attention to the geometry of the space $\mathcal{W}(k,n)$.

It is important to note that the map from admissible Wilson loop diagrams to positroid cells is not injective. It is certainly well defined: by Theorem 2.20, restricting our domain to admissible diagrams ensures that we do always land in a positroid cell, but it is still possible for two different admissible Wilson loop diagrams to give rise to the same positroid cell. As such, the number of positroid cells involved in the definition of $\mathcal{W}(k,n)$ is *strictly fewer* than the number of possible admissible Wilson loop diagrams with k propagators and n vertices.

In order to identify precisely when this happens, we recall the notation introduced in [7].

Definition 2.24. If W is an admissible Wilson loop diagram with a non-empty set of propagators $Q \subseteq \mathcal{P}$ such that

$$|V_Q| = |Q| + 3,$$

then (Q, V_Q) is an *exact subdiagram* of W.

This allows us to define an equivalence relation on admissible Wilson loop diagrams.

Definition 2.25. Two admissible diagrams $W = (\mathcal{P}, n)$ and $W' = (\mathcal{P}', n)$ are equivalent if

1. there exists $Q \subseteq \mathcal{P} \cap \mathcal{P}'$ such that we can write
$$\mathcal{P} = Q \sqcup R \quad \text{and} \quad \mathcal{P}' = Q \sqcup R';$$
2. $V_R = V_{R'}$;
3. the subdiagrams (R, V_R) and (R', V_R) are both unions of exact subdiagrams.

In other words, two admissible diagrams W and W' are equivalent if they differ only by unions of exact subdiagrams supported on the same set of vertices. See Figure 4 for an example of equivalent diagrams.

Theorem 2.26 ([7, Theorem 1.18]). *If $W = (\mathcal{P}, n)$ and $W' = (\mathcal{P}', n)$ are two equivalent admissible Wilson loop diagrams, then $\mathcal{C}(W)$ and $\mathcal{C}(W')$ define the same positroid.*

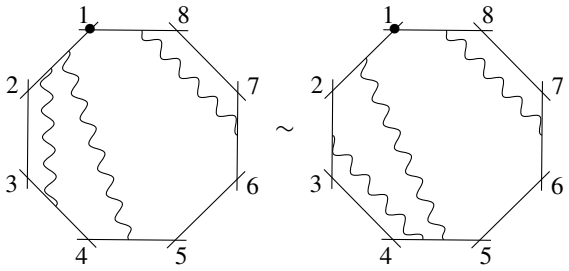

Figure 4. An example of two equivalent diagrams with 3 propagators on 8 vertices.

3. Feynman integrals of WLDs

In this section we give more details on the physical interpretation of Wilson loop diagrams and their associated data, in order to motivate the computations of later sections.

A holomorphic Wilson loop at n points (which we do not define here) is closely related to the n point scattering amplitude of supersymmetric Yang Mills Theory (SYM $N = 4$), see [8]. These Wilson loops $\mathfrak{W}_{k,n}$ are given as sums of Feynman diagrams, which in this setting are the Wilson loop *diagrams* defined in Section 2.2. These diagrams represent interactions in SYM $N = 4$; a diagram with n external vertices and k MHV propagators represents a N^kMHV interaction.

Inspired by the work on the amplituhedron, which interprets the n point N^kMHV on shell scattering amplitude as the volume of a ($4k$-dimensional) subspace of $\mathbb{G}_{\mathbb{R},\geq 0}(k, k+4)$ called the *amplituhedron,* we study the n point N^kMHV scattering amplitude as a (different) volume of the subspace $\mathcal{Z}_*(\mathcal{W}_*(k,n)) \subset \mathbb{G}_{\mathbb{R},\geq 0}(k, k+4)$. We work under the expectation that the $\mathcal{Z}_*(\mathcal{W}_*(k,n))$ is closely related to the amplituhedron. This point of view is different from work done to associate Wilson loop diagrams and the holomorphic Wilson loop to the amplituhedron squared [16]. Namely, in this paper, we are interested in the geometry of the $3k$-dimensional subspace $\mathcal{W}(k,n) \subset \mathbb{G}_{\mathbb{R},\geq 0}(k,n)$ in Definition 2.23.

Note that the amplitude itself is defined on $\mathcal{W}_*(k,n)$; this is described in Sections 3.1 and 3.2 below. However, as seen in Theorem 2.20, the positive structure of the Wilson loop diagrams is encapsulated by the subspace sections $\mathcal{W}(k,n) \subseteq \mathbb{G}_{\mathbb{R},\geq 0}(k,n)$. In Sections 4.3 and 5 below, we examine whether all necessary cancellations to make the theory finite can be verified by considering only the positroid tiling of $\mathcal{W}(k,n)$. We verify this in the case of $\mathbb{G}_{\mathbb{R},\geq 0}(2,6)$ (Theorem 5.1), and conjecture that it holds for general k and n.

3.1. Relating Wilson loops and Wilson loop diagrams

The diagrams we focus on arise from a reformulation of Wilson loops in twistor space [24]. In particular, the equivalent object to a Feynman diagram in this setting is the Wilson loop diagram (WLD). Recall from Section 2.1 that the vertices of the external convex polygon of a WLD correspond to the external particles of an interaction, which we represent as a matrix $\mathcal{Z} \in M_{\mathbb{R},+}(n, k+4)$ with the i-th row (denoted Z_i) corresponding to the i-th vertex. We also consider one additional vector $Z_* \in \mathbb{R}^{4+k}$, which represents a choice of gauge.

Before proceeding, it is worth noting that while twistor space is complex, throughout this paper (and the literature) one speaks of *positivity* in Grassmannians. This is accomplished via a simplification called bosonization, first introduced by Arkani-Hamed [12], and expounded in [16]. Instead of representing the n external Fermionic particles as sections of a complex line bundle over a complex twistor space, we work with a projection, or bosonification, onto a k-dimensional real vector bundle over a 4-dimensional real space-time. That is, we associate to each external particle a vector $Z_i \in \mathbb{R}^{4+k}$, which represents a bosonized Fermion.

Each Z_i is a section of a k-dimensional real vector bundle over twistor space; the first 4 components Z_i^{μ} corresponding to the real momentum data in twistor space, and the last k components corresponding to the bosonized Fermionic data. Without loss of generality, we may choose Z_* to be the 0 section in this bundle., i.e., such that the final k entries of Z_* are 0.

Each propagator depicted in the Wilson loop diagram corresponds to an MHV propagator of the overall interaction. If the propagator p corresponds to the b-th row of the matrix $\mathcal{C}_*(W)$, then it is represented by the vector

$$Y_b = \mathcal{C}_*(W)_b \cdot \mathcal{Z}_* \in \mathbb{R}^{4+k}. \tag{4}$$

Just as a scattering amplitude is given as a sum of Feynman integrals, the holomorphic Wilson loop $\mathfrak{W}_{k,n}(\mathcal{Z})$ is given as a sum of certain integrals $\mathcal{I}(W)(\mathcal{Z}_*)$ associated to Wilson loop diagrams W (see equation (7) below). Given a matrix of external data $\mathcal{Z}_*$ satisfying the conditions of Definition 2.3, the integral $I(W)(\mathcal{Z}_*)$ assigns a volume to the space $\mathcal{C}_*(W) \cdot \mathcal{Z}_*$. The Wilson loop is then given by

$$\mathfrak{W}_{k,n}(\mathcal{Z}) = \sum_{\substack{W \text{admis.} \\ n \text{ point } \mathrm{N}^k\mathrm{MHV diag.}}} \mathcal{I}(W)(\mathcal{Z}_*). \tag{5}$$

For more on the relation between Wilson loop diagrams and traditional Feynman diagrams, see [1]. In particular, the diagrams we consider in this paper correspond to tree level amplitudes (no internal loops). The analysis in this paper can be extended to loop level, but we restrict ourselves to tree level interactions here.

There is one important subtlety to interpreting the holomorphic Wilson loop geometrically as in (5). If two Wilson loop diagrams are equivalent, then they define the same positroid cell, i.e., $\Sigma(W) = \Sigma(W')$. The spaces $\mathcal{C}_*(W)$ and $\mathcal{C}_*(W')$ are therefore also equal. If one were to rewrite the expression in (5) as a sum over distinct subspaces of $\mathcal{W}_*(k,n)$, one would need to sum over volume functionals associated to each subspace:

$$\operatorname{vol} \mathcal{C}_*(W) = \sum_{\substack{W' \text{ s.t.} \\ W' \sim W}} \mathcal{I}(W'). \tag{6}$$

Combining (5) and (6) gives

$$\mathfrak{W}_{k,n} = \sum_{\mathcal{C}_*(W) \subset \mathcal{W}_*(k,n)} \sum_{\substack{W' \text{ s.t.} \\ W' \sim W}} \mathcal{I}(W').$$

In order to study the Wilson loop $\mathfrak{W}_{k,n}$, we need to know exactly which positroids lie in $\mathcal{W}(k,n)$ (the outer summation), how many equivalent diagrams are associated to each positroid (the inner summation), and of course how to compute the integral $\mathcal{I}(W)$ for each WLD W.

3.2. From the Wilson loop diagram W to the integral $\mathcal{I}(W)$

Let $W = (\mathcal{P}, n)$ be an admissible Wilson loop diagram with $|\mathcal{P}| = k$ propagators, and recall the notation for the external data $\mathcal{Z}_*$ given in Section 2.1 above. The integral $\mathcal{I}(W)$ is a functional associated to the space parametrized by $\mathcal{C}_*(W)$: evaluating it on a choice of data $\mathcal{Z}_*$ yields (a component of) the Wilson loop for that particular external data. We define $\mathcal{I}(W)$ as a function of $\mathcal{Z}_*$ as follows [1, 24]:

$$\mathcal{I}(W)(\mathcal{Z}_*) = \int_{\mathbb{R}^{4k}} \frac{\prod_{b=1}^{k} \prod_{a \in V_{p_b}} \mathrm{d}\, c_{b,a}}{R(W)} \delta^{4k|4k}(\mathcal{C}_*(W) \cdot \mathcal{Z}_*), \tag{7}$$

where the $c_{b,a}$ are the entries of the matrix $\mathcal{C}(W)$, and $\delta^{4k|4k}$ and $R(W)$ are given in Definitions 3.1 and 3.2 respectively. An example of the computation of $\mathcal{I}(W)(\mathcal{Z}_*)$ is given in Example 3.3 below.

Definition 3.1. The notation $\delta^{4k|4k}$ is related to the Dirac delta function defined on a vector with both bosonic and Fermion components. Explicitly, we have

$$\delta^{4k|4k}(\mathcal{C}_*(W) \cdot \mathcal{Z}_*) = \prod_{b=1}^{k} (Y_b^{4+b})^4 \delta^4(Y_b^{\mu}), \tag{8}$$

where Y_b are the vectors defined in (4), Y_b^{4+b} is the $(4+b)$-th entry of Y_b, and Y_b^{μ} is the projection of Y_b to its first four entries (as described in Section 2.1).

In order to define the denominator $R(W)$, recall that the vertex labeling of W induces a labeling of the edges, where edge i connects vertex i and $i+1$. For each propagator $p=(i,j)$ in $\mathcal{P}$, define its edge support set to be $E_p=\{i,j\}$. As with the vertex sets, we extend this to any subset $Q\subseteq\mathcal{P}$ by setting $E_Q=\bigcup_{p\in Q}E_p$.

Definition 3.2. If $\{q_1\dots q_s\}$ is the set of propagators incident to the edge i, ordered such that q_1 is the counterclockwise most (closest to the vertex i) and q_s the clockwise most (closest to the vertex $i+1$), define

$$R_i(W)=c_{q_1,i+1}c_{q_s,i}\prod_{m=1}^{s-1}(c_{q_m,i}c_{q_{m+1},i+1}-c_{q_{m+1},i}c_{q_m,i+1}).$$

Note that if i only supports one propagator, then $s=1$ and $R_i(W)=c_{p,i}c_{p,i+1}$. The denominator $R(W)$ is then defined by

$$R(W)=\prod_{e\in E_{\mathcal{P}}}R_e(W).$$

Evaluating $\mathcal{I}(W)$ corresponds to performing the Dirac delta functions $\delta^4(Y_b^\mu)$ and evaluating the expression

$$\frac{\prod_{b=1}^{k}(Y_b^{4+b})^4}{R(W)}$$

at the corresponding points. By (8) this means we should evaluate it at the solution of the system of equations

$$\mathcal{C}_*(W)\cdot\mathcal{Z}_*^\mu=\mathbf{0}.$$

(This process is sometimes called *localizing* the integral at the delta function.)

Since we have an explicit description for the hyperplane on which this occurs (recall equation (3)) we can compute the integral (7) in terms of $\mathcal{Z}_*$ as follows.

We first consider the denominator, writing $R(W)(\mathcal{Z}_*)$ to denote the localization of $R(W)$ at a given choice of external data $\mathcal{Z}_*$. For each edge i of W, we have

$$R_i(W)(\mathcal{Z}_*)=\frac{\sigma_{q_1,i+1}\sigma_{q_s,i}\prod_{m=1}^{s-1}(\sigma_{q_m,i}\sigma_{q_{m+1},i+1}-\sigma_{q_{m+1},i}\sigma_{q_m,i+1})}{\prod_{m=1}^{k}\langle i_{q_m}i_{q_{m+1}}j_{q_m}j_{q_{m+1}}\rangle^2},$$

where $\sigma_{b,a}$ is as in Definition 2.18. Combining this for all edges as above, we obtain

$$R(W)(\mathcal{Z}_*)=\prod_{e\in E_{\mathcal{P}}}R_e(W)(\mathcal{Z}_*).$$

Note that $R(W)(\mathcal{Z}_*)$ is a degree 0 rational function in the determinants $\sigma_{b,a}$ and $\langle i_{p_b}i_{p_b+1}j_{p_b}j_{p_b+1}\rangle$. The *physical* singularities of the theory occur when

$$\langle i_{p_b}i_{p_b+1}j_{p_b}j_{p_b+1}\rangle=0. \tag{9}$$

The simple poles of $\mathcal{I}(W)(\mathcal{Z}_*)$ that occur when either $\sigma_{b,a} = 0$ or $\sigma_{b,a}\sigma_{c,a+1} - \sigma_{c,a}\sigma_{b,a+1} = 0$ are the *spurious* singularities of the theory, and are expected to cancel in the sum in equation (5). There are circumstances under which the various factors of $R(W)(\mathcal{Z}_*)$ are not distinct, in which case $I(W)(\mathcal{Z}_*)$ has poles of higher degree. In this paper, we only consider the simple poles; see Remark 4.10.

In order to examine the numerator of $\mathcal{I}(W)(\mathcal{Z}_*)$, recall from (4) that given a Wilson loop diagram $W = (\mathcal{P}, n)$ with $p_b = (i, j) \in \mathcal{P}$ corresponding to b-th row of $\mathcal{C}_*(W)$, we have

$$Y_p^b = c_{b,i}Z_i^{4+b} + c_{b,i+1}Z_{i+1}^{4+b} + c_{b,j}Z_j^{4+b} + c_{b,j+1}Z_{j+1}^{4+b}.$$

We note that because of the symmetries in the bosonization process, the integral $\mathcal{I}(W)$ is invariant the symmetric group S_k acting on the rows of $\mathcal{C}_*(W)$.

After localization, we obtain

$$F_p^b := (Y_p^b)^4 = \frac{1}{\langle i(i+1)j(j+1)\rangle^4}(\sigma_{b,i}Z_i^{4+b} + \sigma_{b,i+1}Z_{i+1}^{4+b} + \sigma_{b,j}Z_j^{4+b} + \sigma_{b,j+1}Z_{j+1}^{4+b})^4. \tag{10}$$

In other words, the integral $\mathcal{I}(W)$ evaluates to

$$\mathcal{I}(W)(\mathcal{Z}_*) = \frac{\prod_{b=1}^k F_p^b}{R(W)(\mathcal{Z}_*)}. \tag{11}$$

Since SYM $N = 4$ is a finite theory [8, 27], the scattering amplitudes (and thus the holomorphic Wilson loops $\mathfrak{W}_{k,n}$) are finite. However, as seen above, the integrals $\mathcal{I}(W)(\mathcal{Z}_*)$ have spurious poles. In order for these poles to cancel, they must appear on the boundaries of the cells $\Sigma(W)$ and cancel exactly in the induced tiling. This is parallel to the cancellation of poles associated to the BCFW integrals in the amplituhedron calculation [12]. In Section 5 we explicitly show this cancellation for the case $k = 2, n = 6$.

3.3. Example: computing $\mathcal{I}(W)$ for a Wilson loop diagram with $k = 3, n = 8$

Before proceeding with the more geometric aspects of these Wilson loop diagrams, we give an example of the integrals and rational functions involved. As we only consider the case of N^2MHV diagrams, this is a more complicated example than any we consider in the paper, but we include it for give a fuller flavour of the calculations involved. For more example calculations see [19]. In particular, provides a general formula for $\mathcal{I}(W)$ with $k = 1$ and $n \geq 5$.

Example 3.3. Consider the following diagram:

$W =$ 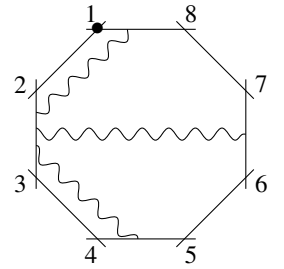

From Definition 2.8, we have

$$C_*(W) = \begin{bmatrix} 1 & c_{1,1} & c_{1,2} & c_{1,3} & 0 & 0 & 0 & 0 & c_{1,8} \\ 1 & 0 & c_{2,2} & c_{2,3} & 0 & 0 & c_{2,6} & c_{2,7} & 0 \\ 1 & 0 & c_{3,2} & c_{3,3} & c_{3,4} & c_{3,5} & 0 & 0 & 0 \end{bmatrix}.$$

Then by the algorithm in Definition 3.2, we obtain

$$R(W) = c_{1,3}(c_{1,2}c_{2,3} - c_{2,2}c_{1,3})(c_{2,2}c_{3,3} - c_{3,2}c_{2,3})c_{3,2}c_{3,4}c_{3,5}c_{2,6}c_{2,7}c_{1,1}c_{1,8}.$$

Localizing the integral against the product of delta functions $\prod_{b=1}^{3} \delta^4(Y_b^\mu)$ as in Definition 3.1 gives

$$\mathcal{C}_*(W)(\mathcal{Z}) = \begin{bmatrix} 1 & \frac{\langle 238* \rangle}{\langle 2381 \rangle} & \frac{\langle *381 \rangle}{\langle 2381 \rangle} & \frac{\langle 2*81 \rangle}{\langle 2381 \rangle} & 0 & 0 & 0 & 0 & \frac{\langle 23*1 \rangle}{\langle 2381 \rangle} \\ 1 & 0 & \frac{\langle *367 \rangle}{\langle 2367 \rangle} & \frac{\langle 2*67 \rangle}{\langle 2367 \rangle} & 0 & 0 & \frac{\langle 23*7 \rangle}{\langle 2367 \rangle} & \frac{\langle 236* \rangle}{\langle 2367 \rangle} & 0 \\ 1 & 0 & \frac{\langle *345 \rangle}{\langle 2345 \rangle} & \frac{\langle 2*45 \rangle}{\langle 2345 \rangle} & \frac{\langle 23*5 \rangle}{\langle 2345 \rangle} & \frac{\langle 234* \rangle}{\langle 2345 \rangle} & 0 & 0 & 0 \end{bmatrix}.$$

By choosing a Z_* with 0 Fermionic components (i.e., with 0 in the final k entries) and assuming that the vectors Z_i^μ are in general position (i.e., that the determinants not involving Z_*^μ are all non-zero), we may evaluate this integral to be

$$\mathcal{I}(W)(\mathcal{Z}_*) = \frac{\mathfrak{Z}_1}{\mathfrak{N}_1} = \frac{\mathfrak{Z}_1}{\mathfrak{N}_1},$$

where

$$\begin{aligned} \mathfrak{Z}_1 &:= (\langle *381 \rangle Z_2^5 + \langle 2*81 \rangle Z_3^5 + \langle 23*1 \rangle Z_8^5 + \langle 238* \rangle Z_1^5)^4 \\ &\quad \cdot (\langle *367 \rangle Z_2^6 + \langle 2*67 \rangle Z_3^6 + \langle 23*7 \rangle Z_6^6 + \langle 236* \rangle Z_7^6)^4 \\ &\quad \cdot (\langle *345 \rangle Z_2^7 + \langle 2*45 \rangle Z_3^7 + \langle 23*5 \rangle Z_4^7 + \langle 234* \rangle Z_5^7)^4, \\ \mathfrak{N}_1 &:= \langle 2*81 \rangle (\langle *281 \rangle \langle 2*67 \rangle - \langle *367 \rangle \langle 2*81 \rangle) \\ &\quad \cdot (\langle *367 \rangle \langle 2*45 \rangle - \langle *345 \rangle \langle 2*67 \rangle) \\ &\quad \cdot \langle *345 \rangle \langle 23*5 \rangle \langle 234* \rangle \langle 23*7 \rangle \langle 236* \rangle \langle 238* \rangle \langle 23*1 \rangle, \end{aligned}$$

and

$$\begin{aligned}\mathfrak{Z}_2 &:= (\sigma_{1,2}Z_2^5 + \sigma_{1,3}Z_3^5 + \sigma_{1,8}Z_8^5 + \sigma_{1,1}Z_1^5)^4 \\ &\quad \cdot (\sigma_{2,2}Z_2^6 + \sigma_{2,3}Z_3^6 + \sigma_{2,6}Z_6^6 + \sigma_{2,7}Z_7^6)^4 \\ &\quad \cdot (\sigma_{3,2}Z_2^7 + \sigma_{3,3}Z_3^7 + \sigma_{3,4}Z_4^7 + \sigma_{3,5}Z_5^7)^4, \\ \mathfrak{R}_2 &:= \sigma_{1,3}(\sigma_{1,2}\sigma_{2,3} - \sigma_{2,2}\sigma_{1,3})(\sigma_{2,2}\sigma_{3,3} - \sigma_{3,2}\sigma_{2,3}) \\ &\quad \cdot \sigma_{3,2}\sigma_{3,4}\sigma_{3,5}\sigma_{2,6}\,\sigma_{2,7}\sigma_{1,1}\sigma_{1,8}.\end{aligned}$$

Notice that this integral has only 10 spurious poles singularities, two of which are defined by the more complicated expressions

$$(\sigma_{1,2}\sigma_{2,3} - \sigma_{2,2}\sigma_{1,3}) \quad \text{and} \quad (\sigma_{2,2}\sigma_{3,3} - \sigma_{3,2}\sigma_{2,3}).$$

If we had instead considered a diagram that did not have propagators sharing a terminal edge, we would have found 12 (i.e., $4k$) spurious poles, each given by a single $\sigma_{b,a}$.

4. The geometry of Wilson loop diagrams representing N^2MHV diagrams at 6 points

We now restrict our attention to the space $\mathcal{W}(2,6)$, which is tiled by cells associated to admissible Wilson loop diagrams with 6 vertices and 2 propagators. The aim of this section is to examine the $\mathcal{W}(2,6)$ case in detail, computing the Le diagrams associated to each WLD, their codimension 1 boundaries, and the homology of the subcomplex in $\mathbb{G}_{\mathbb{R},\geq 0}(2,6)$ whose top-dimensional cells are precisely those in $\mathcal{W}(2,6)$. The case of $\mathcal{W}(1,\geq 5)$ is discussed in [19, Section 3]. Each diagram corresponds to a 3-dimensional positroid cell in $\mathbb{G}_{\mathbb{R},\geq 0}(1,\geq 5)$ where all the spurious singularities of the integral $\mathcal{I}(W)(\mathcal{Z}_*)$ (from equation (7)) cancel on the codimension 1 boundaries shared between the cells.

By computing all possible codimension 1 boundaries shared by pairs of cells in $\mathcal{W}(2,6)$, we also show that the standard diagramatic tool used by physicists to identify shared boundaries of Wilson loop diagrams is insufficient even in this small case, as it does not "see" many of the shared boundaries. This suggests that the combinatorial approach to studying Wilson loop diagrams is a fruitful one.

For simplicity and clarity, we omit the computations underlying the data in this section, but note that they can easily be reconstructed using the vertex-disjoint path

system approach described in Section 2.3.[1] For an algorithm to derive these Le diagrams directly from the Wilson loop diagrams, see [4, Algorithm 3.7].

4.1. The Le diagrams associated to Wilson loop diagrams in $\mathcal{W}(2,6)$

In Table 1 we list the 21 admissible Wilson loop diagrams with 2 propagators on 6 vertices, along with the Le diagram of their associated positroid. We also give each WLD a name ($V_\bullet$, $P_\bullet$, or $E_\bullet$) in order to easily refer to them later. Notice that the rotational symmetry of the Wilson loop diagrams is reflected in the Le diagrams.

Recall from (6) that

$$\mathrm{vol}_{\mathcal{Z}_*}(\mathcal{C}_*(W)\cdot\mathcal{Z}_*) = \sum_{W'\sim W} I(W')(\mathcal{Z}_*).$$

That is, the volume of the space parametrized by matrices $\mathcal{C}_*(W)$ of a Wilson Loop diagram W is given by a sum of integrals associated to all diagrams equivalent to W (including W itself). If W contains an exact subdiagram, then this equivalence class may contain more than one diagram, and thus the volume may involve more than one integral.

Example 4.1. From Table 1, we see that there is an equivalence between each pair of Wilson loop diagrams $E_{i,L}$ and $E_{i,R}$. Indeed, $E_{i,L}$ and $E_{i,R}$ both have two propagators, supported in each case on the set $V_{\mathcal{P}} = [6]\setminus\{i\}$, and these propagators form an exact subdiagram (see Definition 2.24). By Definition 2.25 we therefore have $E_{i,L}\sim E_{i,R}$, and hence by Theorem 2.26 they have the same associated positroid.

In the case of N^2MHV diagrams at 6 points, these are the only non-trivial equivalence classes. These are also the only diagrams that contain exact subdiagrams.

Remark 4.2. There are also six 6-dimensional positroid cells in $\mathbb{G}_{\mathbb{R},\geq 0}(2,6)$ that do not correspond to any Wilson loop diagram. They are listed in Figure 5.

4.2. The geometry of $\mathcal{W}(2,6)$

The spurious singularities of the integrals $\mathcal{I}(W)(\mathcal{Z}_*)$ in equation (7) are conjectured to cancel on the codimension 1 boundaries shared between pairs of cells associated to Wilson loop diagrams. In this section, we use the technology described in Section 2 to establish exactly which cells in $\mathcal{W}(2,6)$ share codimension 1 boundaries in the CW complex of $\mathbb{G}_{\mathbb{R},\geq 0}(2,6)$.

[1] The Python code used by the authors to perform these computations is available as an auxiliary file to this paper on arXiv.

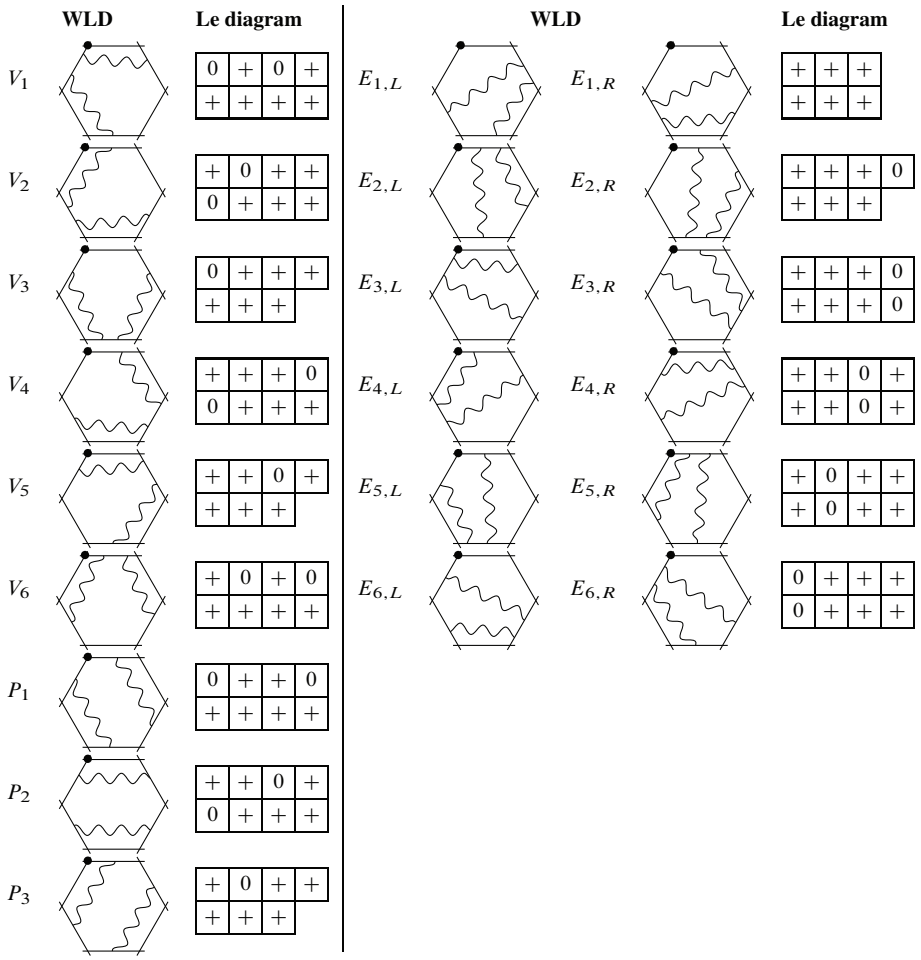

Table 1. All Wilson loop diagrams with $k = 2$ and $n = 6$, and their associated Le diagrams.

In this small and easily computable setting, identifying a shared boundary proceeds as follows. Given two Le diagrams L_1 and L_2, each representing positroid cells of dimension d, we can first obtain their bases sets $\mathcal{B}_1$ and $\mathcal{B}_2$ via the method of vertex-disjoint path systems. Then the cells corresponding to L_1 and L_2 share a $d-1$ dimension boundary if and only if there is a Le diagram L_3 with bases set $\mathcal{B}_3$ such that

(1) L_3 has exactly $d-1$ squares containing a $+$ symbol;

(2) $\mathcal{B}_3 \subset \mathcal{B}_2 \cap \mathcal{B}_1$.

N_1 $\begin{array}{|c|c|c|c|}\hline + & + & 0 & 0 \\ \hline + & + & + & + \\ \hline \end{array}$ N_2 $\begin{array}{|c|c|c|c|}\hline + & 0 & 0 & + \\ \hline + & + & + & + \\ \hline \end{array}$ N_3 $\begin{array}{|c|c|c|c|}\hline 0 & 0 & + & + \\ \hline + & + & + & + \\ \hline \end{array}$

N_4 $\begin{array}{|c|c|c|c|}\hline + & + & + & + \\ \hline 0 & 0 & + & + \\ \hline \end{array}$ N_5 $\begin{array}{|c|c|c|c|}\hline + & + & + & + \\ \hline 0 & + & + \\ \cline{1-3} \end{array}$ N_6 $\begin{array}{|c|c|c|c|}\hline + & + & + & + \\ \hline + & + \\ \cline{1-2} \end{array}$

Figure 5. The 6-dimensional positroid cells in $\mathbb{G}_{\mathbb{R},\geq 0}(2,6)$ that do not correspond to Wilson loop diagrams. As in Table 1, we assign labels to each cell in order to refer to them later.

We now give several examples to illustrate this method, and to highlight the types of behavior exhibited by the cells in $\mathcal{W}(2,6)$.

Example 4.3. Consider the Wilson loop diagrams V_1 and $E_{6,R}$, and their associated positroid cells:

V_1

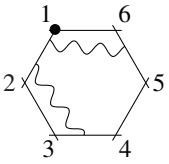

$\begin{array}{|c|c|c|c|}\hline 0 & + & 0 & + \\ \hline + & + & + & + \\ \hline \end{array}$

$\mathcal{B}_{V_1} = \{12, 13, 14, 15, 16, 23, 24, 25, 26, 35, 36, 45, 46\}$

$E_{6,R}$

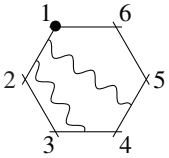

$\begin{array}{|c|c|c|c|}\hline 0 & + & + & + \\ \hline 0 & + & + & + \\ \hline \end{array}$

$\mathcal{B}_{E_{6,R}} = \{12, 13, 14, 15, 23, 24, 25, 34, 35, 45\}$

Drawing on the intuition of vertex-disjoint path systems, it is clear that adding more zeros to a Le diagram (while continuing to respect the Le condition) corresponds to constructing a positroid cell lying on the boundary of the original cell. With this in mind, there is an obvious choice for a codimension 1 boundary shared by V_1 and $E_{6,R}$, namely

$\begin{array}{|c|c|c|c|}\hline 0 & + & 0 & + \\ \hline 0 & + & + & + \\ \hline \end{array}$.

This Le diagram has the basis set $\{12, 13, 14, 15, 23, 24, 25, 35, 45\}$, which is precisely the intersection of $\mathcal{B}_{V_1}$ and $\mathcal{B}_{E_{6,R}}$.

Example 4.4. Now consider the Wilson loop diagrams V_1 and P_1:

V_1

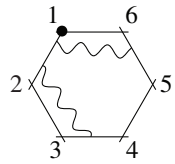

0	+	0	+
+	+	+	+

$\mathcal{B}_{V_1} = \{12, 13, 14, 15, 16, 23, 24, 25, 26, 35, 36, 45, 46\}$

P_1

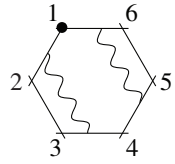

0	+	+	0
+	+	+	+

$\mathcal{B}_{P_1} = \{12, 13, 14, 15, 16, 24, 25, 26, 34, 35, 36, 45, 46\}$

Once again there is an "obvious" codimension 1 boundary:

0	+	0	0
+	+	+	+

,

with bases $\{12, 13, 14, 15, 16, 25, 26, 35, 36, 45, 46\} \subsetneq \mathcal{B}_{V_1} \cap \mathcal{B}_{P_1}$. In fact, V_1 and P_1 share a second codimension 1 boundary, namely

0	+	+	0
+	+	+	0

,

corresponding to the bases set $\{12, 14, 15, 16, 24, 25, 26, 35, 36, 45, 46\}$. This is a manifestation of the same type of behavior highlighted in Example 2.17, and demonstrates why a simpler approach to identifying lower-dimensional boundary cells (e.g., via propagator moves, as in Section 4.3 below, or by constructing Le diagrams "by eye" as in Example 4.3) is insufficient.

Having identified this unexpected second boundary, it is now easy to see (using Table 1) that this boundary is also shared by the cell $\Sigma(E_{3,\bullet})$.

Example 4.5. The 5-dimensional positroid cell corresponding to the Le diagram

0	0	0	+
+	+	+	+

also lies on the boundary of $\Sigma(V_1)$ in $\mathbb{G}_{\mathbb{R},\geq 0}(2, 6)$. However, this 5-dimensional cell does not lie on the boundary of any of the other positroid cells listed in Table 1;

instead, it shares a boundary (in $\mathbb{G}_{\mathbb{R},\geq 0}(2,6)$) with the 6-dimensional cells

$$N_2 = \begin{array}{|c|c|c|c|}\hline + & 0 & 0 & + \\ \hline + & + & + & + \\ \hline \end{array}$$

and

$$N_3 = \begin{array}{|c|c|c|c|}\hline 0 & 0 & + & + \\ \hline + & + & + & + \\ \hline \end{array}.$$

As per Figure 5, neither of these correspond to Wilson loop diagrams.

Therefore, in Examples 4.3 through 4.5, we see that the behavior of boundaries between positroid cells in $\mathbb{G}_{\mathbb{R},\geq 0}(2,6)$ is quite complicated. Certain cells, such as $\Sigma(E_{6,R})$ and $\Sigma(V_1)$ share one codimension 1 boundary between them. Others, such as $\Sigma(V_1)$ and $\Sigma(P_1)$ share two codimension one boundaries between them. Finally, there are sets of 3 cells that share codimension 1 boundaries with each other, for instance $\Sigma(V_1)$, $\Sigma(N_2)$ and $\Sigma(N_3)$.

In $\mathbb{G}_{\mathbb{R},\geq 0}(2,6)$ there are 21 positroid cells of dimension 6 and 50 of dimension 5. From Table 1 we know that 15 of the 6-dimensional cells in $\mathbb{G}_{\mathbb{R},\geq 0}(2,6)$ appear in $\mathcal{W}(2,6)$. Furthermore, from direct computation we find that 38 of the 5-dimensional cells of $\mathbb{G}_{\mathbb{R},\geq 0}(2,6)$ share a boundary with at least two distinct positroid cells associated to Wilson loop diagrams. A further six of the 5-dimensional cells are boundaries of cells $\Sigma(E_i)$, and are thus associated to two different Wilson loop diagrams. The remaining six 5-dimensional cells in $\mathbb{G}_{\mathbb{R},\geq 0}(2,6)$ are each boundaries of precisely one WLD.

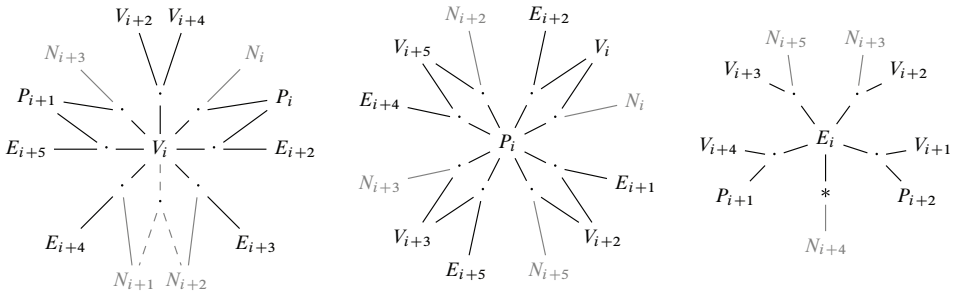

Figure 6. Indices of V_i, E_i, and N_i are taken mod 6, and indices of P_i mod 3. $A - \cdot - B$ indicates that cells A and B share a codimension 1 boundary (represented here by the dot). Dashed gray lines represent boundaries which involve at most one cell associated to an admissible Wilson loop diagram. The solid grey lines correspond to boundaries shared with one of the six 6-dimensional cells of $\mathbb{G}_{\mathbb{R},\geq 0}(2,6)$ that are not associated to Wilson loop diagrams.

Instead of attempting to represent all of these codimension 1 boundaries in one diagram, we describe the shared boundaries of each type of diagram individually; see Figure 6. For visual clarity, we write W in Figure 6 to represent each positroid cell, rather than $\Sigma(W)$. Since $E_{i,L}$ and $E_{i,R}$ correspond to the same positroid cell, we suppress the L or R subscript and simply refer to these cells as E_i.

In Section 5, we show that the spurious singularities of the integrals $\mathcal{I}(W)(\mathcal{Z}_*)$ do cancel exactly on the codimension 1 boundaries shared by pairs of cells associated to Wilson loop diagrams. Figure 6 highlights two types of boundary which will need extra care.

1. The behavior highlighted in Example 4.5 above: a 5-dimensional positroid cell in $\mathbb{G}_{\mathbb{R},\geq 0}(2,6)$ that lies on the boundary of $\Sigma(V_i)$ and is shared with no other Wilson loop diagram. This is represented by the dashed grey lines in Figure 6.
2. The cell labeled $*$ in Figure 6 lies on the boundary of only one cell associated to a Wilson loop diagram, namely the cell $\Sigma(E_{i,\bullet})$, but this cell is associated to two different Wilson loop diagrams: $E_{i,R}$ and $E_{i,L}$.

4.3. A graphical device for understanding codimension one boundaries

In this section we describe how some of the boundaries in Figure 6 can be seen directly from the Wilson loop diagrams.

Definition 4.6. Let $W = (\mathcal{P}, n)$ be an admissible Wilson loop diagram, and $p \in \mathcal{P}$ one of its propagators. For $v \in V_p$, the *boundary propagator* $\partial_v p$ is obtained by moving the endpoint of p away from vertex v while maintaining the requirement that no two propagators cross each other, until one of the following occurs:

1. the endpoint of p reaches another vertex, i.e., $\partial_v p$ is supported on $V_p \backslash v$; or
2. the endpoint of p touches the endpoint of another propagator q.

Define the *boundary diagram* $\partial_{p,v}(W)$ to be the diagram obtained from W by replacing propagator p with $\partial_v p$. We say that $\partial_{p,v}(W)$ is *degenerate* if there is a subset $Q \subset (\mathcal{P} \setminus p) \cup \partial_v p$ such that $|V_Q| < |Q| + 3$.

Example 4.7. Consider the Wilson loop diagram V_1, i.e.,

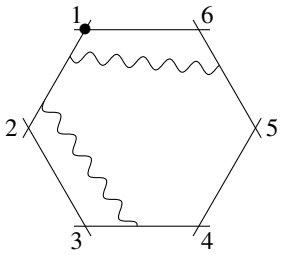

Consider the propagator $p = (1,5)$. By replacing p with $\partial_2 p$ and $\partial_1 p$ respectively, we obtain examples of both types of boundary diagrams:

$\partial_{p,2}(V_1) =$ 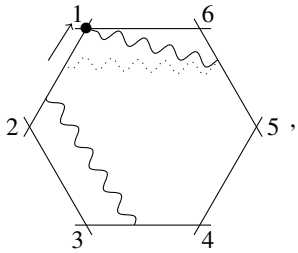

, $\partial_{p,1}(V_1) =$ 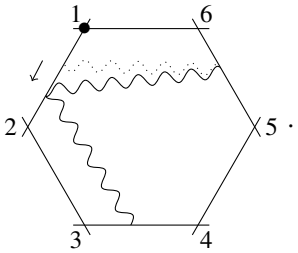

.

Let $q = (1,3)$ be the other propagator in V_1. Clearly $\partial_{p,1}(V_1)$ and $\partial_{q,2}(V_1)$ are (combinatorially) the same diagram; we will not distinguish between them. By considering all possible boundary propagators for V_1, we see that it has 7 distinct boundary diagrams.

Example 4.8. Consider the diagram $E_{6,R}$, which has propagators $p = (1,5)$ and $q = (1,4)$. The boundary $\partial_{p,5}(E_{6,R})$ is degenerate, since the set $\{q, \partial_5 p\}$ is supported on only 4 vertices:

$\partial_{p,5}(E_{6,R}) =$ 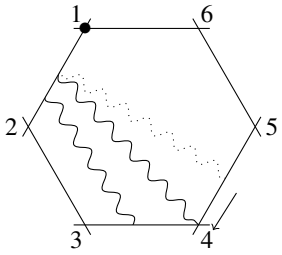

The diagram $\partial_{q,3}(E_{6,R})$ is also degenerate, leaving $E_{6,R}$ with 5 distinct non-degenerate boundary diagrams.

Since the support of a propagator determines which entries of $\mathcal{C}(W)$ are non-zero, we can give an intuitive interpretation of Definition 4.6 in terms of $\mathcal{C}(W)$:

Definition 4.9. Define $\mathcal{C}(\partial_{p,v}(W))$ to be the matrix obtained by applying Definition 2.8 to the diagram $\partial_{p,v}(W)$. In other words, if p is no longer supported on v in $\partial_{p,v}(W)$, then $c_{p,v} = 0$ in $C(\partial_{p,v}(W))$, while if p and q meet in $\partial_{p,v}(W)$ (both lying between vertices v and $v+1$, say) then $c_{q,v}$ and $c_{q,v+1}$ are constrained by the condition that $c_{p,v}c_{q,v+1} - c_{q,v}c_{p,v+1} = 0$ in $\mathcal{C}(\partial_{p,v}(W))$.

We write $\Delta_{p,v}(W)$ for the minor of $\mathcal{C}(W)$ that is set to 0 in $\mathcal{C}(\partial_{p,v}(W))$; that is,

$$\Delta_{p,v}(W) = \begin{cases} c_{p,v} & \text{if } p \text{ is no longer supported on } v \text{ in } \partial_{p,v}(W); \\ c_{p,v}c_{q,v+1} - c_{q,v}c_{p,v+1} & \text{if propagators } p \text{ and } q \text{ touch in } \partial_{p,v}(W). \end{cases}$$

Using this notation, we can write

$$\mathcal{C}(\partial_{p,v}(W)) = \lim_{\Delta_{p,v}\to 0} \mathcal{C}(W).$$

We call $\mathcal{C}(\partial_{p,v}(W))$ a *boundary matrix* of $\mathcal{C}(W)$.

Remark 4.10. By construction, these $\Delta_{p,v}(W)$ are exactly the factors of $R(W)$. In the case of Wilson loop diagrams with 2 propagators and 6 vertices, we may exhaustively check that the factors of $R(W)$ that correspond to degenerate boundaries are exactly those that correspond to non-simple poles of $I(W)(\mathcal{Z}_*)$.

We are now ready to introduce a graphical device for calculating boundaries of Wilson loop diagrams.

Graphical prompt 4.11. *Let $W = (\mathcal{P}, n)$ and $W' = (\mathcal{P}', n)$ be two Wilson loop diagrams. If there exist two vertex propagators pairs (p, v) and (p', v'), with $p \in \mathcal{P}$, $v \in V_p$ and $p' \in \mathcal{P}'$, $v' \in V_{p'}$ such that*

$$\mathcal{C}(\partial_{p,v}(W)) = \mathcal{C}(\partial_{p',v'}(W')),$$

then the corresponding cells $\Sigma(W)$ and $\Sigma(W')$ share a codimension 1 boundary in $\mathbb{G}_{\mathbb{R},\geq 0}(k, n)$.

This is a slightly weaker condition than requiring the boundary diagrams themselves to be equal. Certainly it can happen that two boundary diagrams are equal; for instance, recall the boundary shared between V_1 and $E_{6,R}$ from Example 4.3. In this case, is easy to see that

$$\partial_{(1,5),6}(V_1) = \partial_{(1,4),4}(E_{6,R}),$$

and hence the corresponding matrices $\mathcal{C}(\partial_{(1,5),6}(V_1))$ and $\mathcal{C}(\partial_{(1,4),4}(E_{6,R}))$ are equal as well.

On the other hand, recall the "obvious" boundary between V_1 and P_1 given in Example 4.4: while we do have an equality $\mathcal{C}(\partial_{(1,5),2}(V_1)) = \mathcal{C}(\partial_{(4,6),4}(P_1))$ at the level of the matrices, the boundary diagrams $\partial_{(1,5),2}(V_1)$ and $\partial_{(4,6),4}(P_1)$ are not equal:

$\partial_{(1,5),2}(V_1) =$ 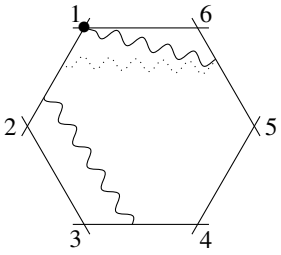

, $\partial_{(4,6),4}(P_1) =$ 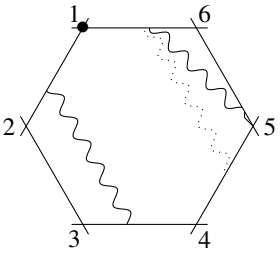

(12)

However, note that the two boundary diagrams only differ in one propagator, and we can obtain one from the other by "sliding" the boundary propagator along half the length of an edge.

Remark 4.12. This "sliding" of the boundary propagator yielding an equivalent diagram is a general phenomenon: if we have two Wilson loop diagrams

$$W = (Q \cup (i, i+2), n) \quad \text{and} \quad W' = (Q \cup (i-1, i+1), n),$$

then the boundary diagrams $\partial_{(i,i+2),i}(W)$ and $\partial_{(i-1,i+1),i+1}(W')$ differ by a half-edge slide and the boundary matrices are equal.

Graphical Prompt 4.11 was originally proposed as a method of identifying all shared boundaries between pairs of admissible Wilson loop diagrams. However, direct computation yields examples of shared boundaries which are *not* seen by this graphical approach. We give two examples to illustrate this phenomenon: Example 4.13, which was already known, and Example 4.14, which was only identified by the authors when they started to systematically apply the tools of total positivity to this question.

Example 4.13. Let p be the propagator $(1, 5)$. This is a propagator present in both V_1 and V_5. Consider the boundary diagrams

$\partial_{p,2}(V_1) =$ 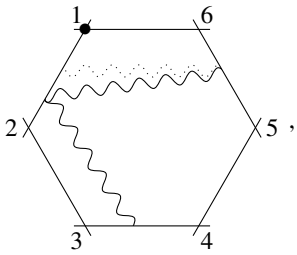

, $\partial_{p,5}(V_5) =$ 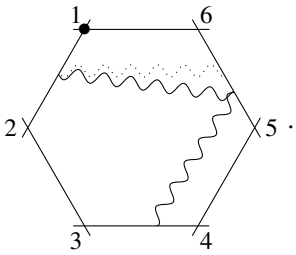

.

The corresponding matrices are

$$C(\partial_{p,2}(V_1)) = \begin{pmatrix} \lambda c_{q,1} & \lambda c_{q,2} & 0 & 0 & c_{p,5} & c_{p,6} \\ c_{q,1} & c_{q,2} & c_{q,3} & c_{q,4} & 0 & 0 \end{pmatrix}$$

and

$$C(\partial_{p,6}(V_5)) = \begin{pmatrix} c_{p,1} & c_{p,2} & 0 & 0 & \mu c_{r,5} & \mu c_{r,6} \\ 0 & 0 & c_{r,3} & c_{r,4} & c_{r,5} & c_{r,6} \end{pmatrix},$$

where $\lambda, \mu \in \mathbb{R}^\times$. Even though these two boundary matrices are not equal, it is easily verified that they have the same sets of independent column vectors. Thus they define the same positroid, and hence the same 5-dimensional cell of $\mathbb{G}_{\mathbb{R},\geq 0}(2,6)$, corresponding to the Le diagram

0	+	0	+
+	+	+	

.

Example 4.14. The positroid cells $\Sigma(V_1)$ and $\Sigma(E_{5,\bullet})$ correspond to the Le diagrams

0	+	0	+
+	+	+	+

and

+	0	+	+
+	0	+	+

respectively. Keeping Example 2.17 in mind, we see that they share a 5-dimensional boundary, namely

+	0	0	+
+	0	+	+

. (13)

This can be realized as the cell associated to a boundary diagram for each of the diagrams V_1, $E_{5,L}$, and $E_{5,R}$, but in a way that is completely missed by the graphical representation. The three boundary diagrams which yield the Le diagram in (13) are

$\partial_{(1,5),5}(V_1) =$

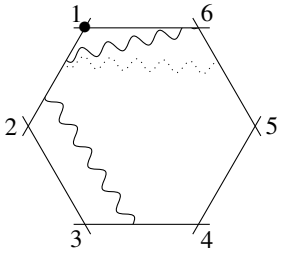

$\partial_{(1,3),3}(E_{5,L}) =$

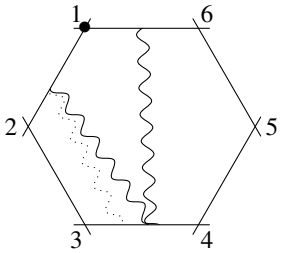

$\partial_{(2,6),3}(E_{5,R}) =$

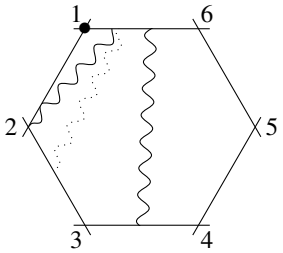

Unlike the example in equation (12), there is no obvious relationship between these three diagrams.

For physicists, only the study of the boundaries obtained via boundary propagators is of interest: they encode the spurious singularities of the integral $\mathcal{I}(W)$. It is therefore important to have a way of identifying all such boundaries.

For the case $k = 2, n = 6$, the following result completely characterizes the shared boundaries obtained from propagator moves.

Proposition 4.15. *B is a 5-dimensional cell in $\mathcal{W}(2,6)$ satisfying $B \subseteq \Sigma(W) \cap \Sigma(W')$ for two distinct Wilson loop diagrams W and W' if and only if*

1. *the cell B can be realized as the cell parametrized by some boundary diagram $\partial_{\hat{p},\hat{v}}(\widehat{W})$, with $\widehat{W}$ an admissible Wilson loop diagram with 2 propagators on 6 vertices;*
2. *the minor $\partial_{\hat{v},\hat{p}}(\widehat{W})$ corresponds to a simple pole of $I(\widehat{W})(\mathcal{Z}_*)$.*

Proof. This is verified by direct calculation, by computing all the 5-dimensional cells contained in $\mathcal{W}(2,6)$ (as shown in Figure 6) and all the boundary diagrams for admissible Wilson loop diagrams with 2 propagators on 6 points. ∎

In light of Proposition 4.15, and preliminary computations for higher k and n, we make the following conjecture.

Conjecture 4.16. *B is a $(3k-1)$-dimensional cell in $\mathcal{W}(k,n)$ satisfying $B \subseteq \Sigma(W) \cap \Sigma(W')$ for two distinct Wilson loop diagrams W and W' if and only if*

1. *the cell B can be realized as the cell parametrized by some boundary diagram $\partial_{\hat{p},\hat{v}}(\widehat{W})$, with $\widehat{W}$ an admissible Wilson loop diagram with k propagators on n vertices;*
2. *the minor $\partial_{\hat{v},\hat{p}}(\widehat{W})$ corresponds to a simple pole of $I(\widehat{W})(\mathcal{Z}_*)$.*

Remark 4.17. $\mathcal{W}(2,6)$ is not simply the 6-skeleton of $\mathbb{G}_{\mathbb{R},\geq 0}(2,6)$. Indeed, each of the cells $\Sigma(V_i)$ admits a boundary in $\mathbb{G}_{\mathbb{R},\geq 0}(2,6)$ which cannot be realized as a the cell of a boundary diagram. These are the dashed gray boundaries seen in Figure 6, which are shared in $\mathbb{G}_{\mathbb{R},\geq 0}(2,6)$ only with cells that do not correspond to admissible Wilson loop diagrams.

Remark 4.18. While the diagrams $E_{i,L}$ and $E_{i,R}$ both give rise to the same cell, Proposition 4.15 indicates that they share a boundary. This is the boundary labeled $*$ in Figure 6, and it will play an important role in Section 5 when we consider the cancellation of spurious poles on codimension 1 boundaries. However, this 5-dimensional cell lies on the boundary of the space $\mathcal{W}(2,6)$, as it is shared by the cells $\Sigma(E_{i,\bullet})$ and $\Sigma(N_{i+4})$ only.

We conclude this section by providing a different interpretation of Example 4.14 in terms of propagator moves. Indeed, to be able to fully graphically predict the geometric relationship between this boundary cell and the Wilson loop diagrams it borders, one needs to step briefly into the world of inadmissible diagrams. We provide

this as an example of the complexity present in the geometry even in this simple case, not to advocate including non-admissible diagrams into the theory.

Example 4.19. Consider the non-admissible Wilson loop diagram

$W' =$ 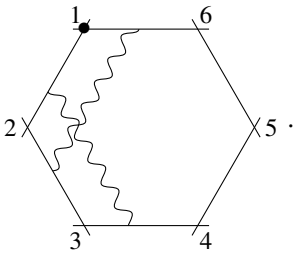

.

Computing the positroid associated with W' yields the cell $\Sigma(E_5)$. Direct computation shows that

$$\mathcal{C}(\partial_{(1,5),5}(V_1)) = \mathcal{C}(\partial_{(2,6),3}(W')),$$

i.e., according to Graphical Prompt 4.11 we would expect V_1 and W' to share a boundary. Indeed, if we draw the two boundary diagrams we obtain

$\partial_{(1,5),5}(V_1) =$ 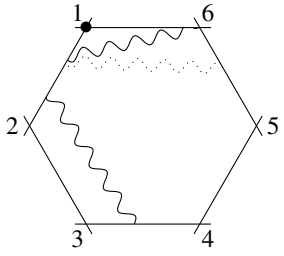

$\sim$ 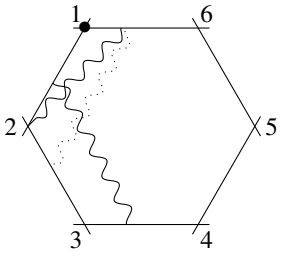

$= \partial_{(2,6),3}(W'),$

i.e., the two diagrams are related by the same "half-edge slide" propagator move seen in equation (12).

Diagrams with crossing propagators are meaningless from a physical point of view, but this suggests they may be a useful tool to study the combinatorics and geometry of Wilson loop diagrams in the future.

4.4. The homology of $\mathcal{W}(2,6)$

Figure 6 gives an insight into the geometry of the space $\mathcal{W}(2,6)$. In this section, we discuss the geometry in more detail and compute the homology of this space. Note that this is *not* the cohomology of the amplituhedron. Nor is it the homology of the larger space $\mathcal{W}_*(2,6)$ that is conjectured to be the preimage of the amplituhedron. We only consider the positive subspace $\mathcal{W}(2,6)$ tiled by the positroid cells.

Recall from Section 3 that the Wilson loop diagrams define a subspace $\mathcal{W}_*(2,6) \subseteq \mathbb{G}_{\mathbb{R}}(2,7)$ parametrized by the matrices $\mathcal{C}_*(W)$. The external data $\mathcal{Z}_* \in M(7,6)$ defines a projection

$$\mathcal{Z}_*\colon \mathbb{G}_{\mathbb{R}}(2,7) \to \mathbb{G}_{\mathbb{R},\geq 0}(2,6),$$

that can be restricted onto the subspace $\mathcal{W}_*(2,6)$. The holomorphic Wilson loop

$$\mathfrak{W}_{2,6} = \sum_{\substack{W \text{ admis.,} \\ \text{2 props., 6 verts.}}} \mathcal{I}(W)(\mathcal{Z}_*)$$

assigns a volume to the projection $\mathcal{Z}_*(\mathcal{W}_*(2,6))$.

Recall from Definition 2.23 that

$$\mathcal{W}(2,6) = \bigcup_{\substack{W \text{ admis.,} \\ \text{2 props., 6 verts.}}} \overline{\Sigma(W)}.$$

The Le diagrams associated to these cells are listed in Table 1. By counting the $+$ symbols in each Le diagram, we see that $\mathcal{W}(2,6)$ is a 6-dimensional submanifold of $\mathbb{G}_{\mathbb{R},\geq 0}(2,6)$. The following facts about $\mathcal{W}(2,6)$ follow by direct computation.

1. There are six 6-dimensional cells in $\mathbb{G}_{\mathbb{R},\geq 0}(2,6)$ that are not part of $\mathcal{W}(2,6)$. These are denoted N_i in Figure 5.
2. Also, there are six 5-dimensional cells in $\mathbb{G}_{\mathbb{R},\geq 0}(2,6)$ lying on the boundaries between N_i and N_{i+1} which are also not in $\mathcal{W}(2,6)$.
3. All other cells of dimension ≤ 5 in $\mathbb{G}_{\mathbb{R},\geq 0}(2,6)$ are contained in $\mathcal{W}(2,6)$.
4. The manifold $\mathcal{W}(2,6)$ is not closed. The boundary of the manifold consists of exactly the twelve 5-dimensional cells indicated in Figure 6 that are shared by exactly one cell defined by a Wilson loop diagram and a cell N_i.

While there are several conjectures about the homology of the amplituhedron [11], there is little know about the preimage of this space before the projection imposed by the external particle data, either in the BCFW or Wilson loop context. With the data described above in hand, we are able to compute the homology of $\mathcal{W}(2,6)$ directly.

Theorem 4.20. *The homology groups of $\mathcal{W}(2,6)$ are as follows:*

$$H_i(\mathcal{W}(2,6)) = \begin{cases} \mathbb{R} & \text{if } i \in 0,5, \\ 0 & \text{else.} \end{cases}$$

Proof. This result was obtained by direct computation, using Python and Sympy [25] to obtain the basis sets for each positroid and to compare each pair of basis sets, and the Chain Complexes module of the computer algebra system Sage [26] to compute the homology. The code used by the authors is provided as an auxiliary file on arXiv. ∎

The homology calculation for $\mathcal{W}(1, \geq 5)$, is more straightforward, and can be calculated by hand. Namely, every cell corresponding to a diagram in $\mathcal{W}(2, \geq 5)$ shares at most one boundary with another cell corresponding to another diagram in set. Furthermore, every codimension one boundary of said cell is a codimension one boundary of exactly one other such cell.

Theorem 4.21. *The homology groups of $\mathcal{W}(2,n)$ with $n \geq 5$ are as follows:*

$$H_i(\mathcal{W}(1,n)) = \begin{cases} \mathbb{R} & \text{if } i \in 0,3 \\ 0 & \text{else.} \end{cases}$$

Proof. First note the Le diagram associated to any diagram of the form

$$W_{i,j} = ((i,j),n)$$

has the form

0	…	0	+	+	0	…	0	+	if $j < n$,
+	0	…	0	+	+	0	…	0	if $j = n$,

where the Le diagram fits inside a $1 \times n-1$ box. If $j < n$ there are $n-i$ boxes, with plusses in the $n-j$, $n-(j+1)$ and $n-i$ boxes, counted from the left. If $j = n$ there are $n-1$ boxes, with plusses in the first, $n-i$ and $n-(i+1)$ boxes, counted from the left. Note, this implies that the cells $\Sigma(W_{i,j})$ are all 3-dimensional.

Second, note from [19, Section 3] that if $j > i+1$ and $i > j+1$ in the cyclic ordering on $[n]$, the cell corresponding to the diagram $W_{i,j} = ((i,j),n)$, i.e., $\Sigma(W_{i,j})$ shares a boundary with the cells $\Sigma(W_{(i+1,j)})$, $\Sigma(W_{i-1,j})$, $\Sigma(W_{i,j+1})$ and $\Sigma(W_{i,j-1})$. Otherwise, without loss of generality, assume $j = i+1$. This diagram shares a boundary with the cells $\Sigma(W_{(i+1,j+1)})$, $\Sigma(W_{i-1,j})$, $\Sigma(W_{i,j+1})$ and $\Sigma(W_{i-1,j-1})$. Direct calculation from the Le diagrams above show that these are all the codimension 1 boundaries of each of these cells.

Since $n \geq 5$, for any $W_{i,j} \in \mathcal{W}(1,n)$, $\Sigma(W_{i,j})$ shares exactly one codimension one boundary with exactly one other cell of the form $\Sigma(W_{l,m})$. This fact, along with the cyclic nature of the boundary sharing means that the cohomology is as desired by direct calculation. ∎

5. The cancellation of spurious poles

In this section, we return to the question posed in Section 3: verifying that the spurious singularities of the Wilson loop diagrams with 2 propagators on 6 points cancel in the holomorphic Wilson loop calculation given in (5). For a direct calculation of the cancellation of spurious singularities for $k = 1$ and $n \geq 5$, see [19, Section 3].

Recall from Proposition 4.15 that in $\mathcal{W}(2,6)$

1. the non-degenerate boundaries $\partial_{p,v}(W)$ correspond to degree one factors of $R(W)(\mathcal{Z}_*)$, that is, spurious poles of $\mathcal{I}(W)(\mathcal{Z}_*)$ (these poles are denoted $\Delta_{p,v}(W)$);
2. the limits $\lim_{\Delta_{p,v}(W)\to 0} C(W)$ correspond exactly to the codimension 1 boundaries of $\Sigma(W)$ that are shared with some cell $\Sigma(W')$ with $W' \neq W$. (Recall that while the Wilson loop diagrams W and W' are different, their corresponding positroid cells may be the same.)

In this section, we prove the following theorem.

Theorem 5.1. *Let W be an admissible Wilson loop diagram in with 2 propagators and 6 external particles. Let Σ' be any 5-dimensional boundary of the 6-dimensional cell $\Sigma(W)$. Then*

$$\sum_{\substack{\partial_{p,v}(W')=\Sigma' \\ W' \text{ admiss.}}} \operatorname*{Res}_{\Delta_{p,v}(W')\to 0} \mathcal{I}(W')(\mathcal{Z}_*) = 0. \tag{14}$$

In other words, we show that the residues of $\operatorname{Res}_{\Delta_{p,v}(W)\to 0} \mathcal{I}(W)(\mathcal{Z}_*)$ cancel exactly on the 5-dimensional cells $\lim_{\Delta_{p,v}(W)\to 0} C(W)$. A direct corollary of this is that the sum of the spurious poles cancel in the sum

$$\mathfrak{W}_{2,6} = \sum_{\substack{W \text{ admiss.} \\ n \text{ verts}, k \text{ props}}} \mathcal{I}(W)(\mathcal{Z}_*)$$

We begin with an outline of the proof, which is proved in three cases.

Case 1 considers the types of propagators moves described in Section 4.3. In this simplest case, we consider two Wilson loop Diagrams $W = (\{p,q\},6)$ and $W' = (\{p',q\},6)$, where p and p' are such that $\mathcal{C}(\partial_{p,v}(W)) = \mathcal{C}(\partial_{p',v'}(W'))$. For

a picture of the type of computations considered in this case, see Example 4.4. This case captures the boundary between P_i and V_i, V_{i+2}, V_{i+3}, or V_{i+5}; the boundaries between P_i and $E_{i+1,L}$, $E_{i+2,R}$, $E_{i+4,L}$, or $E_{i+5,R}$; the boundaries between V_i and $E_{i-1,R}$ or $E_{i+2,L}$; and the boundaries between $E_{i,R}$ and $E_{i,L}$ indicated in Figure 6. The fact that $\Sigma(E_{i,R}) = \Sigma(E_{i,L})$ then explains why certain triples of the form $\Sigma(P_i)$, $\Sigma(E_j)$ and $\Sigma(V_k)$ share a common boundary.

Case 2 considers what happens when bringing together two propagators on a boundary edge. In this case, one is not simply setting a single parameter to 0, but instead setting a 2×2 minor of $\mathcal{C}(W)$ to 0. The actual calculation for this case requires a change of basis in the integral. For a picture of the type of computations considered in this case, see Example 4.13. This accounts for the three way boundary between V_i, V_{i+2} and V_{i+4} indicated in Figure 6.

Case 3 handles the type of boundary highlighted in Example 4.14. As shown in that example, there are two spurious poles of $\mathcal{I}(V_i)$, namely $\Delta_{(i,i-2),i-2}(V_i)$ and $\Delta_{(i,i+2),i+2}(V_i)$, that correspond to a 5-dimensional boundary of the cells $\Sigma(E_{i-2})$ and $\Sigma(E_{i-3})$ respectively. However, the fact that this boundary sits between these two cells is missed by Graphical Prompt 4.11, indicating that something more complicated is happening here. For a picture of the type of computations considered in this case, see Example 4.14.

Proof of Theorem 5.1. Recall from (11) that for $W = (\{p, q\}, 6)$, the integral $\mathcal{I}(W)$ localized at $\mathcal{Z}_*$ is given by

$$\mathcal{I}(W)(\mathcal{Z}_*) = \frac{F_p^1 F_q^2}{R(W)(\mathcal{Z}_*)},$$

where the F_p^b are defined in (10), and $R(W)(\mathcal{Z}_*)$ is computed directly after Definition 3.2. The proof proceeds by considering the three cases outlined above. Inspection of Figure 6 shows that these cases are exhaustive.

Case 1. In this case, there exist a pair of Wilson loop diagrams $W = (\{p, q\}, 6)$ and $W' = (\{p', q\}, 6)$ such that $\mathcal{C}(\partial_{p,v}(W)) = \mathcal{C}(\partial_{p',v'}(W'))$. After localization, we have $\Delta_{v,p}(W) = \sigma_{p,v}$ and $\Delta_{v',p'}(W') = \sigma_{p',v'}$. Notice that $|V_p \cap V_{p'}| = 3$, and that $\{v\} = V_p \backslash V_{p'}$ and $\{v'\} = V_{p'} \backslash V_p$. In this case, it follows from the definition of $\sigma_{b,a}$ that

$$\sigma_{p,v} = -\sigma_{p',v'}.$$

Also, in the limit $\sigma_{p,v} \to 0$, we may write Z_*^μ as a linear combination of the Z_w^μ with $w \in V_p$. That is,

$$Z_*^\mu = \sum_{w \in V_p; w \neq v} \alpha_w Z_w^\mu, \quad \alpha_w \in \mathbb{R}. \tag{15}$$

In this limit, for any $w \in V_p \cap V_{p'}$, it follows from (15) that

$$\sigma_{p,w} = \alpha_w \langle i_p(i_p+1)\, j_p(j_p+1)\rangle$$

and

$$\sigma_{p',w} = -\alpha_w \langle i_{p'}(i_{p'}+1)\, j_{p'}(j_{p'}+1)\rangle.$$

We can use this to write

$$\lim_{\sigma_{p,v}\to 0} F_p^1 = \Big(\sum_{w\in V_p\cap V_{p'}} \alpha_w Z_w^\mu\Big)^4 \langle i_p(i_p+1)\, j_p(j_p+1)\rangle^4.$$

Similarly,

$$\lim_{\sigma_{p',v'}\to 0} F_{p'}^1 = \Big(\sum_{w\in V_p\cap V_{p'}} -\alpha_w Z_w^\mu\Big)^4 \langle i_{p'}(i_{p'}+1)\, j_{p'}(j_{p'}+1)\rangle^4.$$

Therefore, after making the above substitutions at the appropriate limits, one sees exactly that

$$\lim_{\sigma_{p,v}\to 0} (\mathcal{I}(W)(\mathcal{Z}_*)) = -\lim_{\sigma_{p',v'}\to 0} (\mathcal{I}(W')(\mathcal{Z}_*)).$$

Case 2. In this case, and the next, one needs to first perform a careful change of variables before localization. Then one may proceed by calculations in the same vein as in Case 1. In this case, we consider what happens when bringing two propagators to meet on an edge, as in the boundary diagram $\partial_{(i,i+4),i}(V_i)$ for example. We begin by rewriting the matrices $\mathcal{C}_*(V_i)$, $\mathcal{C}_*(V_{i+2})$ and $\mathcal{C}_*(V_{i-2})$ such that the minors $\Delta_{i,(i,i+4)}(V_i)$, $\Delta_{i+2,(i+2,i)}(V_{i+2})$ and $\Delta_{i-2,(i-2,i+2)}(V_{i-2})$ can each be expressed by a single variable. In other words, we chose $\alpha, \alpha_+, \alpha_-, f, f_+$ and f_- to be real variables such that

$$\mathcal{C}_*(V_i) = \begin{bmatrix} 1 & \cdots & c_{1,i} & c_{1,i+1} & \cdots \\ 1 & \cdots & \alpha c_{1,i} & \alpha c_{1,i+1} + f_+ & \cdots \end{bmatrix},$$

$$\mathcal{C}_*(V_{i+2}) = \begin{bmatrix} 1 & \cdots & c_{1,i+2} & c_{1,i+3} & \cdots \\ 1 & \cdots & \alpha_+ c_{1,i+2} & \alpha_+ c_{1,i+3} + f_- & \cdots \end{bmatrix},$$

$$\mathcal{C}_*(V_{i-2}) = \begin{bmatrix} 1 & \cdots & c_{1,i-2} & c_{1,i-1} & \cdots \\ 1 & \cdots & \alpha_- c_{1,i-2} & \alpha_- c_{1,i-1} + f & \cdots \end{bmatrix}.$$

Under this notation, the common 5-dimensional cell, $\Sigma(V_i) \cap \Sigma(V_{i+2}) \cap \Sigma(V_{i-2})$, can be represented by the limit

$$\lim_{f\to 0} \mathcal{C}_*(V_i) = \lim_{f_+\to 0} \mathcal{C}_*(V_{i+2}) = \lim_{f_-\to 0} \mathcal{C}_*(V_{i-2}).$$

Rewriting the integrals $\mathcal{I}(V_i)(\mathcal{Z}_*)$ under this new parametrization, we obtain

$$\mathcal{I}(V_i) = \int \frac{\mathrm{d}\, c_{1,i-2}\, \mathrm{d}\, c_{1,i-1}\, \mathrm{d}\, c_{1,i}\, \mathrm{d}\, c_{1,i+1}\, \mathrm{d}\, \alpha\, \mathrm{d}\, f\, \mathrm{d}\, c_{2,i+2}\, \mathrm{d}\, c_{2,i+3}}{c_{1,i-2}c_{1,i-1}c_{1,i}c_{1,i+1}\alpha f c_{2,i+2}c_{2,i+3}} \delta^{8|8}(\mathcal{C}_*(V_i)\cdot \mathcal{Z}_*),$$

$$\mathcal{I}(V_{i+2})(\mathcal{Z}_*) = \int \frac{\mathrm{d}\, c_{1,i}\, \mathrm{d}\, c_{1,i+1}\, \mathrm{d}\, c_{1,i+2}\, \mathrm{d}\, c_{1,i+3}\, \mathrm{d}\, \alpha_+\, \mathrm{d}\, f_+\, \mathrm{d}\, c_{2,i+4}\, \mathrm{d}\, c_{2,i+5}}{c_{1,i}c_{1,i+1}c_{1,i+2}c_{1,i+3}\alpha_+ f_+ c_{2,i+4}c_{2,i+5}} \delta^{8|8}(\mathcal{C}_*(V_{i+2})\cdot \mathcal{Z}_*),$$

$$\mathcal{I}(V_{i-2})(\mathcal{Z}_*) = \int \frac{\mathrm{d}\, c_{1,i-2}\, \mathrm{d}\, c_{1,i-1}\, \mathrm{d}\, c_{1,i}\, \mathrm{d}\, c_{1,i+1}\, \mathrm{d}\, c_{2,i-4}\, \mathrm{d}\, c_{2,i-3}\, \mathrm{d}\, \alpha_-\, \mathrm{d}\, f_-}{c_{1,i-2}c_{1,i-1}c_{1,i}c_{1,i+1}c_{2,i-2}c_{2,i-3}\alpha_- f_-} \delta^{8|8}(\mathcal{C}_*(V_{i-2})\cdot \mathcal{Z}_*).$$

In the above calculation, since the respective boundaries send the 2×2 minors $\Delta_{i,(i,i+4)}(V_i)$, $\Delta_{i+2,(i+2,i)}(V_{i+2})$, and $\Delta_{i-2,(i-2,i+2)}(V_{i-2})$ to 0, one cannot employ the computational trick of (15) to compare F_p^1 to $F_{p'}^1$. Therefore, we need to introduce a change of parametrization of $\mathcal{C}_*(V_{i+2})$ and $\mathcal{C}_*(V_{i-2})$. Given an appropriate choice of ordering of the propagators of each diagram,[2] define

$$\mathcal{C}'_*(V_{i+2}) = \begin{bmatrix} \frac{-\alpha_+}{1-\alpha_+} & \frac{1}{1-\alpha_+} \\ 1 & 0 \end{bmatrix} \mathcal{C}_*(V_{i+2}). \tag{16}$$

and

$$\mathcal{C}'_*(V_{i-2}) = \begin{bmatrix} 1 & 0 \\ \frac{-\alpha_-}{1-\alpha_-} & \frac{1}{1-\alpha_-} \end{bmatrix} \mathcal{C}_*(V_{i-2}). \tag{17}$$

Notice that the matrices $\lim_{f_+\to 0}\mathcal{C}'_*(V_{i+2})$ and $\lim_{f_-\to 0}\mathcal{C}'_*(V_{i-2})$ have the same form as $\lim_{f\to 0}\mathcal{C}_*(V_i)$. That is, all three matrices have 0s, 1s and variables in the same entries.

Let $\mathcal{I}(\mathcal{C}'_*(V_{i+2}))$ and $\mathcal{I}(\mathcal{C}'_*(V_{i-2}))$ be the two integrals $\mathcal{I}(V_{i+2})$ and $\mathcal{I}(V_{i-2})$ rewritten in terms of the variables entries of $\mathcal{C}'_*(V_{i+2})$ and $\mathcal{C}'_*(V_{i-2})$ respectively. Evaluating these integrals (as in Case 1, or as demonstrated explicitly in Example 3.3), we get that

$$\lim_{f_+\to 0}\mathcal{I}(V_{i+2})\lim_{f_+\to 0}\mathcal{I}(\mathcal{C}'_*(V_{i+2})) = \frac{-1}{1-\sigma_{2,i}/\sigma_{1,i}}\lim_{f\to 0}\mathcal{I}(V_i)$$

[2]Note that this process requires a choice of ordering on the propagators of V_i. We use the convention that the propagator $(j, j+2)$ defines the second row of the matrix $C_*(V_j)$ for $j = i$ or $j = i+2$, while the same propagator defines the first row of the associated matrix when $j = i-2$.

and

$$\lim_{f_-\to 0} \mathcal{I}(V_{i-2}) \lim_{f_-\to 0} \mathcal{I}(\mathcal{C}'_*(V_{i-2})) = \frac{\sigma_{2,i}/\sigma_{1,i}}{1-\sigma_{2,i}/\sigma_{1,i}} \lim_{f\to 0} \mathcal{I}(V_i).$$

Therefore, $\lim_{f\to 0} \mathcal{I}(V_i) + \lim_{f_+\to 0} \mathcal{I}(V_{i+2}) + \lim_{f_-\to 0} \mathcal{I}(V_{i-2}) = 0$, as desired.

Case 3. The final case is very similar to the second case, but with a different change of variables which exploits the fact that $\Sigma(E_{i,R}) = \Sigma(E_{i,L})$. The purpose of this change of variables is to write $\mathcal{I}(E_{i,R})$ and $\mathcal{I}(E_{i,L})$ under a common parametrization of this cell, and thus associate a single integral to it. We introduce a new matrix $\mathcal{C}_*(E_i)$, given by

$$\mathcal{C}_*(E_i) = \begin{bmatrix} 1 & \cdots & c_{1,i+1} & c_{1,i+2} & c_{1,i+3} & c_{1,i+4} & 0 & \cdots \\ 1 & \cdots & 0 & c_{2,i+2} & c_{2,i+3} & c_{2,i+4} & c_{2,i+5} & \cdots \end{bmatrix},$$

where the $c_{b,a}$ are real variables as usual. Note that this matrix is yet another parametrization of the cell $\Sigma(E_i)$. Write

$$\mathcal{I}(\mathcal{C}_*(E_i)) = \int_{(\mathbb{R}^4)^2} \frac{\mathfrak{Z}_3}{\mathfrak{N}_3} \delta^{8|8}(C_*(E_i)\cdot \mathcal{Z}_*),$$

where

$$\begin{aligned} \mathfrak{Z}_3 &:= \mathrm{d}\, c_{1,i+1}\, \mathrm{d}\, c_{1,i+2}\, \mathrm{d}\, c_{1,i+3}\, \mathrm{d}\, c_{1,i+4}\, \mathrm{d}\, c_{2,i+2}\, \mathrm{d}\, c_{2,i+3}\, \mathrm{d}\, c_{2,i+4}\, \mathrm{d}\, c_{2,i+5}, \\ \mathfrak{N}_3 &:= c_{1,i+1}c_{2,i+5}c_{2,i+2}c_{1,i+4}(c_{1,i+2}c_{2,i+3} - c_{2,i+2}c_{1,i+3}) \\ &\quad \cdot (c_{1,i+3}c_{2,i+4} - c_{1,i+4}c_{2,i+3}). \end{aligned}$$

By direct calculations of the form employed in Case 1, we see that

$$\begin{aligned} \lim_{\sigma_{1,i+4}\to 0} \mathcal{I}(\mathcal{C}_*(E_i))(\mathcal{Z}_*) &= -\lim_{c_{(i,i+2),i}\to 0} \mathcal{I}(V_{i+2}), \\ \lim_{c_{2,i+2}\to 0} \mathcal{I}(\mathcal{C}_*(E_i)) &= -\lim_{c_{(i+3,i+5),i}\to 0} \mathcal{I}(V_{i+3}). \end{aligned}$$

However, $\mathcal{I}(\mathcal{C}_*(E_i))$ is a different integral than either $\mathcal{I}(E_{i,R})$ or $\mathcal{I}(E_{i,L})$. The rest of this proof proceeds by showing that

$$\mathcal{I}(\mathcal{C}_*(E_i)) = \mathcal{I}(E_{i,R}) + \mathcal{I}(E_{i,L}).$$

We proceed by a change of variables as in Case 2. We rewrite the integrals $\mathcal{I}(E_{i,R})$ and $\mathcal{I}(E_{i,L})$ in terms of the parametrization of $\Sigma(E_i)$ given by the matrix $\mathcal{C}_*(E_i)$. As before, we fix an ordering of the propagators in both $\mathcal{C}_*(E_{i,R})$ and $\mathcal{C}_*(E_{i,L})$. Let

the first row of both matrices correspond to the propagator $(i+1, i+4)$. Under this choice of ordering, write

$$\mathcal{C}'_*(E_{i,R}) = \begin{bmatrix} 0 & 1 \\ \frac{c_{2,i+1}}{c_{2,i+1}-c_{1,i+1}} & \frac{-c_{1,i+1}}{c_{2,i+1}-c_{1,i+1}} \end{bmatrix} \mathcal{C}_*(E_{i,R})$$

and

$$\mathcal{C}'_*(E_{i,L}) = \begin{bmatrix} \frac{c_{2,i-1}}{c_{2,i-1}-c_{1,i-1}} & \frac{-c_{1,i-1}}{c_{2,i-1}-c_{1,i-1}} \\ 0 & 1 \end{bmatrix} \mathcal{C}_*(E_{i,L}).$$

Under these changes of variables, the matrices $\mathcal{C}'_*(E_{i,R})$ and $\mathcal{C}'_*(E_{i,L})$ have the same form as $\mathcal{C}_*(E_i)$. That is, they all have 0s, 1s and variables in the same positions.[3] Let $\mathcal{I}(\mathcal{C}'_*(E_{i,R}))$ and $\mathcal{I}(\mathcal{C}'_*(E_{i,L}))$ be the integrals $\mathcal{I}(E_{i,R})$ and $\mathcal{I}(E_{i,R})$ written in terms of the variables in the parametrization $\mathcal{C}_*(E_i)$. By performing the appropriate changes of variables (as in Case 2), we obtain

$$\mathcal{I}(\mathcal{C}'_*(E_{i,R})) + \mathcal{I}(\mathcal{C}'_*(E_{i,L})) = \mathcal{I}(\mathcal{C}_*(E_i)),$$

as required. ∎

Corollary 5.2. *All spurious poles cancel out in the sum*

$$\mathfrak{W}_{2,6} = \sum_{\substack{W \text{ admiss.} \\ n \text{ verts, } k \text{ props}}} \mathcal{I}(W)(\mathcal{Z}_*).$$

Proof. This follows directly from Theorem 5.1. ∎

Remark 5.3. There are 6 cells (each lying on the boundary of a cell of the form $\Sigma(V_i)$), that do not appear in the calculations of Theorem 5.1 at all. These are precisely the 5-dimensional cells which cannot be realized as cells associated to boundary diagrams of Wilson loop diagrams.

6. The intricate structure of cancellation

We conclude with a discussion of some of the structure of the geometry of the Wilson loop diagrams uncovered by the calculation performed in this paper, and outline the future work needed to fully understand this structure. Note that the case of $k = 1$,

[3] The interested reader is invited to multiply out the expressions for $\mathcal{C}'_*(E_{i,\bullet})$ and verify this for themselves!

$n \geq 5$, contemporaneously explained in [19], is simpler and does not reveal these structures.

For instance, in this paper, we show that in there are positroid cells that are associated to multiple Wilson loop diagrams, and that, in this case, both these diagrams are needed in order to perform the calculation of spurious poles. In order to make further progress on understanding the cancellation of spurious poles, it is necessary to understand the structure of these postroid cells and characterize the associated Wilson loop diagram. In [7, Theorem 1.18] the authors give a characterization of which diagrams define the same positroid cell. In subsequent work, [3, Theorem 3.25], the authors show that these are the only diagrams corresponding to the same cells. Furthermore, [3, Corrollary 3.16] counts the number of Wilson loop diagrams associated to each cell. Without this context, one cannot generalize the phenomenon observed here that $E_{i,R}$ and $E_{i,L}$ both correspond to the same positroid cell (see Table 1). This is necessary both to generalize the cancellation and the cohomology result.

In this paper, we observe that not all boundaries of Wilson loop diagrams correspond to those given by Graphical Prompt 4.11 as previously conjectured. In order to understand the boundaries, one needs to develop a means of translating between the Wilson loop diagrams to the Grassmann necklace and Le diagram of $\Sigma(W)$. This is done in two stages in subsequent work. First, in [4, Algorithm 3.7] gives an algorithm to translate a Wilson loop diagram to the correct Grassmann Necklace. Then, [2, Algorithm 2] translates from Grassmann necklaces to Le diagrams. However, aside from this algorithm, this algorithm identifies the positroid cell associated to each Wilson loop diagram. To date, there is no algorithmic manner to identify the boundaries on which each spurious pole vanishes.

Furthermore, in order to generalize the cancellation of singularities, one first needs a better understanding of the geometry of the vanishing locus of the polynomial $R(W)$. The structure of the polynomial $R(W)$ is understood in subsequent work, [4, Proposition 5.3], where the authors discover that the polynomial $R(W)$ is the product of the square free factors of the minors of the matrix $C(W)$ defined by the elements of the Grassmann necklace of $\Sigma(W)$. This has the advantage of implying that the factors of $R(W)$ vanish on the boundary of the cells $\Sigma(W)$ [5, Proposition 3.11]. In order to ensure cancellation of singularities on the boundaries, one needs to consider the vanishing locus of the factors of $R(W)$ on the boundaries. Subsequent work, [5, Theorem 3.12], shows that, for factors with codimension one vanishing locus, the vanishing locus is dense in the appropriate boundary. This work also shows that in the general codimension one cancellation calculation, one only needs to consider contributions of either two or three diagrams for each factor.

While the calculations of this paper are only concerned with the cancellation of codimension one spurious singularities. However, there are also spurious singularities, as shown in this paper, that have higher codimension. To date, there are no results

about the cancellation of higher order singularities. In fact, identifying which factors of $R(W)$ give rise to higher codimension singularities is only possible due to the subsequently published work: [23, Theorem 3.2] and [5, Theorem A.8].

In order to compute the cohomology of the geometric subspace of $\mathbb{G}_{\mathbb{R},\geq 0}(k,n)$ defined by general $\mathcal{W}(k,n)$, one needs to know the dimension of the cells $\Sigma(W)$. Though conjectured to be $3k$, this is shown in subsequent work, [23, Theorem 3.2] or [4, Theorem 4.12].

Finally, one cannot compute a general cohomology of this subspace without understanding when the subspace defined by $\mathcal{W}(k,n)$ is an open manifold (e.g., in $\mathcal{W}(2,6)$) and when it is not (e.g., $\mathcal{W}(1,\geq 5)$). In particular, one needs to classify when there are cells $\Sigma(W)$ that have a codimension boundary that is not shared with a cell defined by another Wilson loop diagrams, as illustrated by the N_i in Figure 6. In [5] there is some characterization of this phenomenon, but it is by no means complete.

Acknowledgements. The work on this paper was begun during the conference "Total Positivity: A Bridge Between Representation Theory and Physics" hosted by the University of Kent, and both authors are grateful for the opportunities and connections sparked by it.

Agarwala is indebted to Paul Heslop and Alastair Stewart for many critical discussions about integrals associated to Wilson loop diagrams. Some of the calculational maneuvers used to compare integrals along boundaries presented in this paper come directly from examples worked out in correspondences and conversations with them.

Fryer gratefully acknowledges the hospitality of the University of Kent mathematics department, who provided a welcoming and supportive environment on several occasions during the writing of this paper, and thanks Matthew Towers for providing an easy-to-code algorithm for testing containment between positroid cells.

References

[1] T. Adamo and L. Mason, MHV diagrams in twistor space and the twistor action. *Phys. Rev. D* **86** (2012), no. 6, article id. 065019

[2] S. Agarwala and S. Fryer, An algorithm to construct the Le diagram associated to a Grassmann necklace. *Glasg. Math. J.* **62** (2020), no. 1, 85–91 Zbl 1436.05024 MR 4039001

[3] S. Agarwala, S. Fryer, and K. Yeats, Combinatorics of the geometry of Wilson loop diagrams I: equivalence classes via matroids and polytopes. *Canad. J. Math.* **74** (2022), no. 4, 1177–1208 Zbl 07570457 MR 4464584

[4] S. Agarwala, S. Fryer, and K. Yeats, Combinatorics of the geometry of Wilson loop diagrams II: Grassmann necklaces, dimensions, and denominators. *Canad. J. Math.* **74** (2022), no. 6, 1625–1672 Zbl 07632803 MR 4520663

[5] S. Agarwala and C. Marcott, Cancellation of spurious poles in $N = 4$ SYM: physical and geometric. 2021, arXiv:2105.00541

[6] S. Agarwala and C. Marcott, Wilson loops in SYM $\mathcal{N} = 4$ do not parametrize an orientable space. *Ann. Inst. Henri Poincaré D* **8** (2021), no. 4, 583–622 Zbl 1483.81130 MR 4337449

[7] S. Agarwala and E. Marin-Amat, Wilson loop diagrams and positroids. *Comm. Math. Phys.* **350** (2017), no. 2, 569–601 Zbl 1359.81133 MR 3607457

[8] L. F. Alday and J. Maldacena, Gluon scattering amplitudes at strong coupling. *J. High Energy Phys.* (2007), no. 6, article id. 064 MR 2326587

[9] F. Ardila, F. Rincón, and L. Williams, Positroids and non-crossing partitions. *Trans. Amer. Math. Soc.* **368** (2016), no. 1, 337–363 Zbl 1325.05015 MR 3413866

[10] N. Arkani-Hamed, J. Bourjaily, F. Cachazo, A. Goncharov, A. Postnikov, and J. Trnka, *Grassmannian geometry of scattering amplitudes*. Cambridge University Press, Cambridge, MA, 2016 Zbl 1365.81004 MR 3467729

[11] N. Arkani-Hamed, H. Thomas, and J. Trnka, Unwinding the amplituhedron in binary. *J. High Energy Phys.* (2018), no. 1, article id. 016

[12] N. Arkani-Hamed and J. Trnka, The amplituhedron. *J. High Energy Phys.* **2014,** no. 10, article id. 030 Zbl 1468.81075

[13] R. Boels, L. Mason, and D. Skinner, From twistor actions to MHV diagrams. *Phys. Lett. B* **648** (2007), no. 1, 90–96 Zbl 1248.81133 MR 2304197

[14] M. Bullimore, L. Mason, and D. Skinner, Twistor-strings, Grassmannians and leading singularities. *J. High Energy Phys.* (2010), no. 3, article id. 070 Zbl 1271.81101 MR 2653460

[15] K. Casteels, A graph theoretic method for determining generating sets of prime ideals in quantum matrices. *J. Algebra* **330** (2011), 188–205 Zbl 1273.17016 MR 2774624

[16] B. Eden, P. Heslop, and L. Mason, The correlahedron. *J. High Energy Phys.* (2017), no. 9, article id. 156 Zbl 1382.81139 MR 3710458

[17] P. Galashin, S. N. Karp, and T. Lam, The totally nonnegative Grassmannian is a ball. *Sém. Lothar. Combin.* **80B** (2018), article id. 23 Zbl 1417.05253 MR 3940598

[18] K. R. Goodearl, S. Launois, and T. H. Lenagan, Torus-invariant prime ideals in quantum matrices, totally nonnegative cells and symplectic leaves. *Math. Z.* **269** (2011), no. 1-2, 29–45 Zbl 1234.16018 MR 2836058

[19] P. Heslop and A. Stewart The twistor Wilson loop and the amplituhedron. *J. High Energy Phys.* (2018), no. 10, article id. 142 Zbl 1402.81244 MR 3879742

[20] A. Hodges, Eliminating spurious poles from gauge-theoretic amplitudes. *J. High Energy Phys.* (2013), no. 5, article id. 135 Zbl 1342.81291 MR 3080526

[21] S. N. Karp and L. K. Williams, The $m = 1$ amplituhedron and cyclic hyperplane arrangements. *Int. Math. Res. Not. IMRN* (2019), no. 5, 1401–1462 Zbl 1429.52024 MR 3920352

[22] S. N. Karp, L. K. Williams, and Y. X. Zhang, Decompositions of amplituhedra. *Ann. Inst. Henri Poincaré D* **7** (2020), no. 3, 303–363 Zbl 1470.81048 MR 4152617

[23] C. Marcott, Basis shape loci and the positive Grassmannian. 2019, arXiv:1904.13361

[24] L. Mason and D. Skinner, The complete planar S-matrix of $\mathcal{N} = 4$ SYM as a Wilson loop in twistor space. *J. High Energy Phys.* (2010), no. 12, article id. 018 Zbl 1294.81122 MR 2818481

[25] A. Meurer, C. P. Smith, M. Paprocki, O. Čertík, S. B. Kirpichev, M. Rocklin, A. Kumar, S. Ivanov, J. K. Moore, S. Singh, T. Rathnayake, S. Vig, B. E. Granger, R. P. Muller, F. Bonazzi, H. Gupta, S. Vats, F. Johansson, F. Pedregosa, M. J. Curry, A. R. Terrel, Š. Roučka, A. Saboo, I. Fernando, S. Kulal, R. Cimrman, and A. Scopatz, SymPy: symbolic computing in Python. *PeerJ Computer Science* (2017), 3:e103

[26] J. H. Palmieri, Chain complexes module in SageMath. The Sage Mathematics Software System, v. 7.2 https://doc.sagemath.org/html/en/reference/homology/sage/homology/chain_complex.html

[27] S. Parke and T. Taylor, Amplitude for n-gluon scattering. *Phys. Rev. Lett.* **56** (1986), no. 23, 2459–2460

[28] A. Postnikov, Total positivity, Grassmannians, and networks. 2006, arXiv:math/0609764

[29] A. Postnikov, D. Speyer, and L. Williams, Matching polytopes, toric geometry, and the totally non-negative Grassmannian. *J. Algebraic Combin.* **30** (2009), no. 2, 173–191 Zbl 1264.20045 MR 2525057

[30] K. Rietsch and L. Williams, Discrete Morse theory for totally non-negative flag varieties. *Adv. Math.* **223** (2010), no. 6, 1855–1884 Zbl 1206.57044 MR 2601003

[31] K. Talaska, A formula for Plücker coordinates associated with a planar network. *Int. Math. Res. Not. IMRN* (2008), article id. rnn081 Zbl 1170.05031 MR 2439562

Communicated by Adrian Tanasă

Received 19 April 2020; revised 9 May 2021.

Susama Agarwala
Mathematics Department, United States Naval Academy, Chauvenet Hall,
572C Holloway Road, Annapolis, MD 21402-5002, USA; susama@alum.mit.edu

Siân Zee Fryer
Department of Mathematics, University of California, South Hall, Room 6607, Santa Barbara,
CA 93106-3080, USA; sianfryer@math.ucsb.edu